This is a preprint, the final version is subject to change, of the American Mineralogist (MSA)
Cite as Authors (Year) Title. American Mineralogist, in press.
(DOI will not work until issue is live.) DOI: http://dx.doi.org/10.2138/am.2014.4726

Ms 4726 REVISION 1

A New UHP Metamorphic Complex In The ~1.8 Gya Nagssugtoqidian Orogen Of West Greenland

William E. Glassley[1,2], John A. Korstgård[2], Kai Sørensen[3] and Steen W. Platou[4]

[1]Department of Geology, University of California, Davis, California 95616, U.S.A.

[2]Department of Geoscience, Aarhus University, 8000 Århus C, Denmark

[3]Geological Survey of Denmark and Greenland (GEUS), Copenhagen, Denmark

[4]Deceased

Abstract

The Nagssugtoqidian Orogen is a ca. 1.8 Gya belt of east-west trending, highly deformed rocks that bisects central Greenland. Although a variety of data have suggested this belt marks the location of a continent-continent collision zone, evidence of subduction has been lacking. We report here mineralogical evidence from four samples within a well-defined lithologic unit of metabasic and metasedimentary ocean floor rocks of a previously unrecognized UHP metamorphic episode. The UHP episode is recorded by remnants of orthopyroxene exsolved from majoritic garnet, graphitized diamond, exsolution of rutile from garnet and pyroxenes, exsolution of magnetite from olivine, and complex exsolution textures in ortho- and clinopyroxenes (including omphacite). Associated with these mineralogical features is an unusual occurrence of quartz needles in Mn-rich fayalite. From textural characteristics, we infer that the quartz needles

Always consult and cite the final, published document. See http://www.minsocam.org or GeoscienceWorld

This is a preprint, the final version is subject to change, of the American Mineralogist (MSA)
Cite as Authors (Year) Title. American Mineralogist, in press.
(DOI will not work until issue is live.) DOI: http://dx.doi.org/10.2138/am.2014.4726

exsolved from the fayalite. To our knowledge, olivine with exsolved silica has not been reported. We note, however, that experimental studies have shown that β-spinel can incorporate excess silica. We therefore speculate these quartz needles may be silica that exsolved from Mn-rich ahrensite, the Fe analogue of ringwoodite, upon decompression and inversion to fayalite. If correct, this occurrence would be the first reported sample of naturally occurring olivine (fayalite) that inverted from ahrensite. Corroborating an early UHP history are reaction relationships that delineate a path through high-pressure and high temperature conditions during decompression. P-T conditions inferred for the UHP episode are ~ 7 GPa at ~975 ^{o}C. The unusually low T for this UHP system at ~1.8 Gya may reflect either very rapid subduction rates at that time, or unexpectedly cool mantle conditions. Preservation of the UHP assemblages probably is due, in large part, to the exceptionally low a_{H2O} during decompression and cooling. These UHP rocks establish that the location of the subduction and suture zones that must have existed prior to and during the collision of continents was along what is now the northern edge of the Nordre Strømfjord shear zone.

Keywords: UHP metamorphism, majorite, diamonds, Nagssugtoqidian, pigeonite, ahrensite, Paleoproterozoic, exsolution

Always consult and cite the final, published document. See http://www.minsocam.org or GeoscienceWorld

This is a preprint, the final version is subject to change, of the American Mineralogist (MSA)
Cite as Authors (Year) Title. American Mineralogist, in press.
(DOI will not work until issue is live.) DOI: http://dx.doi.org/10.2138/am.2014.4726

INTRODUCTION

Since the first discovery (Chopin 1984) of coesite in alpine metamorphic rocks, ultra-high pressure (UHP) metamorphism has been recognized in more than twenty localities around the world (see summaries in Chopin, 2003, and Ernst and Liou, 2008). All of these sites are within metamorphic terrains younger than 1,000 million years, reflecting the rarity of preserving mineral assemblages that are inherently highly thermodynamically unstable. Even though rare and of minuscule areal extent, these sites have profoundly affected conceptual models of global geodynamic processes, and have raised important new questions regarding the behavior of continental crust during continent-continent collisions, the representativeness of modern day tectonic structures and collisions, and the mechanics of subduction and exhumation (Ernst and Liou, 2008). However, recognizing such sites is fraught with challenges. In most instances the remnant mineralogy providing evidence of UHP metamorphism is preserved only at the micron scale, and is ambiguous unless associated with multiple UHP indicators.

We report here multiple lines of evidence that establish the presence of a UHP metamorphic complex in the Nordre Strømfjord shear zone (NSSZ), which is located within the Nagssugtoqidian Mobile Belt of West Greenland. Prior to this discovery, this mobile belt had been considered a classic example of upper amphibolite to granulite facies deep crustal regional metamorphism (Davidson, 1979; Hansen, 1979; Glassley and

Sørensen, 1980; Glassley, 1983; Mengel, 1983). Although that regional metamorphic model does reflect the last significant metamorphic event these rocks experienced, the UHP mineralogy we describe here unequivocally demonstrates that, for at least some of the lithologies within the NSSZ, a significant chapter in the metamorphic history has been missed.

In addition, these results demonstrate that the metamorphic and tectonic processes that result in UHP metamorphism extend at least as far back as ca. 1.8 Gya. Finally, we report observations that may be evidence of the first terrestrial example of Fe-rich ringwoodite in a UHP terrain.

GEOLOGIC SETTING

The Nagssugtoqidian Orogen (NO) is a ca. 200 km wide complex of variably deformed rocks that extend across southern Greenland (Fig. 1). This belt lies along the northern margin of the main Archaean block in south Greenland and is divided into lithologically coherent belts that are separated by major shear zones (Escher, 1970; Bak et al., 1975a,b; Korstgård, 1979 and papers therein; Garde and Kalsbeek, 2006 and papers therein). The most northern shear zone is the Nordre Strømfjord shear zone (NSSZ) (Bak et al., 1975a; Sørensen, 1983).

Kalsbeek et al (1987) were the first to propose that the NO “contains a cryptic suture between two once separate Archaean plates”. This concept was based on 1) their interpretation of a ca. 1921 My calc-alkaline complex as an oceanic arc remnant and 2)

This is a preprint, the final version is subject to change, of the American Mineralogist (MSA)
Cite as Authors (Year) Title. American Mineralogist, in press.
(DOI will not work until issue is live.) DOI: http://dx.doi.org/10.2138/am.2014.4726

the presence of Paleoproterozoic metasediments that were metamorphosed and deformed around 1850 my and which are interleaved with Archaean rocks. However, they noted that "the suture itself has not been located", although they speculated that the suture lay southeast of the NSSZ.

Over the following 15 years a growing body of field, chemical and isotopic data documented that the period of calc-alkaline igneous activity persisted for about 50 my (1920-1870 my). This work also demonstrated that several belts of predominantly Paleoproterozoic supracrustal rocks are present within the mobile belt, among them supracrustal rocks within the NSSZ (Kalsbeek and Nutman, 1996; Scott et al., 1998; Whitehouse et al., 1998; Nutman et al., 1999; Connelly and Mengel, 2000; Connelly et al., 2000; van Gool et al., 2002).

Metamorphism within this orogeny was dated at 1860-1840 Mya, with late stage metamorphic mineral growth extending to ca. 1780 Mya (Hickman and Glassley, 1984; Kalsbeek et al., 1987; Taylor and Kalsbeek, 1990; Kalsbeek and Nutman, 1996; Connelly et al., 2000; Willigers et al., 2001; Mazur et al., 2012), and has been interpreted to be the last consequence of continent-continent suturing. Maximum metamorphic conditions, based on a variety of geothermometers and geobarometers, were reported to be ca. 800^{o}C – 850^{o}C and ca. 1.0 GPa (Davidson, 1979; Hansen, 1979; Glassley and Sørensen, 1980; Glassley, 1983; Mengel, 1983; Mazur et al., 2012).

Always consult and cite the final, published document. See http://www.minsocam.org or GeoscienceWorld

Glassley et al. (2007) reported discovery of a high-pressure mineral assemblage (sample 492042E, a garnet-olivine-spinel-clinopyroxene gneiss; T ca. 785^{o}C and P ca. 21 kb) located within a mapped supracrustal belt (Fig.1) in the western portion of the NSSZ and near its northern border, indicating that the metamorphic history of this region was likely more complex than hitherto assumed. However, although indicative of unusually high pressures, sample 492042E, in and of itself, could not provide a definitive answer to the "cryptic suture" enigma of Kalsbeek et al. (1987).

Following discovery and analysis of sample 492042E, we re-examined hundreds of thin sections archived at Aarhus University from mapping campaigns in the late 1960's and 1970's. Two additional samples were identified that contained the metamorphic mineral assemblage garnet-olivine (123220, collected by Steen Platou in 1969; and 159966 collected by Flemming Mengel and Kai Sørensen in 1976). These were collected approximately 30 km west-southwest of sample 492042E and, like it, were within supracrustal units along and near the northern shear zone border. Two additional samples of striking mineralogy (540521b and 540599) were collected by us in 2012 in an area within a few kilometers of the location of sample 123220 (Figs. 1 and 2). The remainder of this paper describes the mineralogy and P-T history of these four samples.

ANALYTICAL METHODS

Electron microprobe analyses: All of the analyses reported here were conducted at electron microprobe (EMP) facilities at Aarhus University, Denmark and the University

This is a preprint, the final version is subject to change, of the American Mineralogist (MSA)
Cite as Authors (Year) Title. American Mineralogist, in press.
(DOI will not work until issue is live.) DOI: http://dx.doi.org/10.2138/am.2014.4726

of California, Davis, USA. The EMP at Aarhus University is a JEOL JXA 8200. The EMPA at UC Davis is a Cameca SX-100. Both instruments have 5 wavelength-dispersive, computer driven spectrometers for quantitative analyses and an EDS capability for qualitative analyses. Analyses at both facilities were conducted using the same protocol, i.e., an accelerating potential of 15 kV, and a beam current of between 10 and 20 nA, using natural, well characterized mineral standards and matrix matching. Spot size was varied, depending upon mineral properties, in order to avoid beam damage and minimize volatilization. The raw data were corrected for deadtime, drift and matrix effects using standard commercial software specific to each instrument.

Raman spectra were obtained using a Renishaw RM1000 Research Laser Raman Microscope at the Keck Spectral Imaging Facility at the University of California, Davis. Excitation of the sample was accomplished using an argon-ion laser (514 nm; 2.4121 ev). A 25% transmission filter provided about 500uW in the laser spot using a 50X objective. Raman signals were collected through hard laser filters (dual holographic Rayleigh filters), providing access to the Stokes side of the Raman emission. Spectral analysis was conducted using the GRAMS spectra analysis application (from Thermo Scientific) The spectra presented here were slightly smoothed using 2-point running averages.

In-situ quadrupole LA-ICP-MS analyses were performed using a Photon Instruments laser ablation sample introduction system coupled to an Agilent 7700 ICP-MS. NIST 612 was used as a calibration standard and NIST 610 was incorporated in the sample run to test data reproducibility. NIST 612 and NIST 610 standards were analyzed

Always consult and cite the final, published document. See http://www.minsocam.org or GeoscienceWorld

This is a preprint, the final version is subject to change, of the American Mineralogist (MSA)
Cite as Authors (Year) Title. American Mineralogist, in press.
(DOI will not work until issue is live.) DOI: http://dx.doi.org/10.2138/am.2014.4726

158 twice at the beginning and twice at the end of the sample run. Laser spots were located in
159 close proximity to previous electron microprobe (EMP) analyses. Calcium results from
160 the corresponding EMP analyses were used as an internal standard. A laser spot size of
161 65 microns was used for each point analysis. The laser was operated at 50% power, 10
162 Hz repetition rate, and fluence of 4.45 joules/cm^2. Each spot was ablated and measured
163 for 25 seconds, with a pause of 90 seconds between analyses to allow purging of the
164 spectrometer and baseline stabilization. ICP-MS output data were corrected and
165 converted into part-per-million (ppm) concentrations using Iolite data reduction software
166 (Paton et al., 2011).
167 The nomenclature and abbreviations for minerals follows that of Whitney and
168 Evans (2010) unless otherwise noted.
169

170 **RESULTS**

171 Samples 123220, 159966 and 540521b occur within belts of complexly
172 interleaved rocks that are mapped as undifferentiated metasedimentary/metavolcanic
173 rocks and amphibolite (Map Sheet Agto 67 V 1.Nord, 1:100,000; 1987; Fig. 1). Sample
174 540599 is a single garnet crystal (approximately 6 cm x 5 cm) that was plucked from a
175 quartzo-feldspathic garnet-sillimanite-graphite schist a few hundred meters southwest
176 from 540521b. Large (maximum dimensions of up to 10 cm) garnet porphyroblasts made
177 up in excess of 60 volume percent of the outcrop of this unit. This schist bounds the
178 southern edge of the metasedimentary/metavolcanic and amphibolite unit from which the
179 other samples were collected.
180

Always consult and cite the final, published document. See http://www.minsocam.org or GeoscienceWorld

Samples 123220 and 159966 are coarse-grained olivine (Ol)-garnet (Grt)-clinopyroxene (Cpx)-orthopyroxene (Opx)-quartz (Qtz) gneisses with graphite (Gph), magnetite (Mag) and ilmenite (Ilm). A very weak fabric is defined by slight elongation of Grt, preferred orientation of pigeonite (Pgt) (123220) and weak compositional layering. Sample 540521b is a coarse-grained garnet pyroxenite with Ilm.

The bulk rock compositions of 123220 and 540521b (Table 1) are part of a suite of seven samples that have the highest Fe and Mn compositions within a database of 219 bulk rock analyses we have assembled. The other characteristics of this suite are low SiO_2 (< 45%), low alkalis ($Na_2O + K_2O < 1.0\%$), low MgO (0.95% to 4.95%), low Al_2O_3 (0.46 to 3.88%) and high MnO/MgO (0.25 to > 7). These rocks are identical chemically and mineralogically to eulysites, which were first thoroughly described by Tilley (1936) from western Scotland. They are interpreted as being deposited by ocean floor exhalative hydrothermal processes (Coats et al., 1996). Sample 159966, of which only a polished thin section remains, is likely to belong to the same suite of ocean floor exhalative metasediments, based on the similarity of the mineral compositions (discussed below) to those in 123220.

Majoritic Garnet

Two generations of garnets can be observed in samples 123220, 159966 and 540521b. Small, groundmass garnets that are usually inclusion free are associated with late-stage, granulite facies metamorphism. These small garnets post-date larger, elongate

This is a preprint, the final version is subject to change, of the American Mineralogist (MSA)
Cite as Authors (Year) Title. American Mineralogist, in press.
(DOI will not work until issue is live.) DOI: http://dx.doi.org/10.2138/am.2014.4726

to sub-idiomorphic, porphyroblastic garnets that are up to 0.5 cm in diameter. These earlier garnets are the subject of the remainder of this section.

The first generation garnets possess clear cores, inclusion-filled mantles and clear rims (Fig. 3). They are all spessartine-rich almandines (ca. 80 mole % spessartine + almandine), with 1-5 mole % pyrope and 15-17 mole % grossular (Table 1).

EMP analyses of the larger garnets (Fig. 4a,b) exhibit consistent zoning patterns in which the cores are Fe-rich. Outward from the cores, the inner mantle region exhibits Ca and Mn increases at the expense of Fe and Mg, but the outer mantles tend to reverse this trend with an increase in Fe and Mg. Clear, thin outer rims are enriched in Mn at the expense of other cations.

LA-ICPMS analysis shows the cores to be Cr- and Ti-rich, relative to mantles and rims (Fig. 4c). These analyses also indicate a systematic zoning in the rare earth elements (REE) in which the cores are strongly depleted in LREE while the mantle zone is consistently enriched (by about 10x to 100x; Fig. 4d) in LREE.

The inclusions in the mantle regions are numerous and diverse. They are usually a few microns to a few tens of microns in size and are commonly the locus of decompression cracks. In samples 123220 and 159966, inclusions of apatite, Mg-, Mn- and Fe-carbonates, monazite, rutile and ilmenite are dispersed irregularly throughout the mantles. Ilmenites, however, also occur as clusters of parallel blades and rods, which is a

Always consult and cite the final, published document. See http://www.minsocam.org or GeoscienceWorld

This is a preprint, the final version is subject to change, of the American Mineralogist (MSA)
Cite as Authors (Year) Title. American Mineralogist, in press.
(DOI will not work until issue is live.) DOI: http://dx.doi.org/10.2138/am.2014.4726

morphology suggestive of exsolution, but for which other evidence is lacking. An Al-Si phase, possibly kyanite, was observed in several inclusions, but could not be positively identified because of secondary alteration. Carbon inclusions (Fig. 3a,b) are predominately graphite, but contain relict diamond, based on Raman spectral analysis (see discussion of Raman analysis below). In sample 540521b inclusions are mainly ilmenite + qtz, aligned in well-defined trains (Fig. 3c,d).

The most abundant and systematically distributed inclusions in 123220 and 159966, however, exhibit unequivocal exsolution morphologies (Fig. 3b). These inclusions occur as clusters of aligned rhombohedral forms a few microns to ten microns in diameter. High resolution, 3D optical image processing (Fig. 3b) shows them to be aligned in three directions that are consistent with a {111} garnet structure orientation.

Although the morphologies of the inclusions in 123220 and 159966 are identical, the inclusions in 123220 have been altered and oxidized and reliable EMP analyses of them could not be obtained. Inclusions in 159966, although altered to finely intergrown mats of Cl-bearing hydrous phases, preserve systematic compositional characteristics that allow reconstruction of their original composition.

More than 80 spot analyses of the hydrated inclusions in 159966 were obtained. Of these, two thirds were short, multi-spot traverses across individual inclusions. Despite some scatter, three consistent compositions were observed in these analyses (Fig. 5). On

Always consult and cite the final, published document. See http://www.minsocam.org or GeoscienceWorld

248 the basis of the population statistics for each group, an anhydrous composition was
249 computed, assuming an oxygen basis of 6:
250
251 $$(Ca_{0.03}Mg_{0.09}Mn_{0.14}Fe_{1.73})_{1.99}(Al_{0.02}Si_{1.99})_{2.01}O_6.$$
252
253 For comparison, the average unaltered Opx in 159966 has the stoichiometry:
254
255 $$(Ca_{0.06}Mg_{0.24}Mn_{0.23}Fe_{1.50})_{2.03}(Al_{0.01}Si_{1.97})_{1.98}O_6,$$
256
257 which is poorer in Fe and richer in Mg, Ca and Mn. These results are consistent with one
258 Raman spectrum collected from an inclusion in porphyroblastic garnet in sample 159966
259 that had sharp, well-defined peaks matching precisely a ferrosilite standard (RRUFF data
260 base number R070387). Using variable focus optical microscopy, the measured minimum
261 volume of the Opx inclusions in the garnet was 4.0 % with a most likely value 6.0. %.
262
263 In contrast to the inclusions in 123220 and 159966, the inclusions in 540521b
264 occur as distinct trains that, at low magnification, define rod-like forms (Fig. 3c) that are
265 consistently oriented parallel to the {111} direction of the garnets, based on their
266 relationship to the idiomorphic form of the clear garnet cores. At higher magnification
267 (Fig. 3d,e) the inclusions that define the rod-like forms are seen to invariably be 2-phase
268 Qtz-Ilm grains. The proportion of the two phases is always the same, to the extent that
269 can be determined optically. These characteristics require that these inclusion trains once
270 were continuous, single-phase needle-like rods that segmented during recrystallization,

This is a preprint, the final version is subject to change, of the American Mineralogist (MSA)
Cite as Authors (Year) Title. American Mineralogist, in press.
(DOI will not work until issue is live.) DOI: http://dx.doi.org/10.2138/am.2014.4726

likely driven by surface-energy minimization requirements. Additionally, upon segmentation, the individual grains must have consisted of a homogeneous phase that later decomposed to the bi-mineral assemblage Ilm and Qtz. The original exsolved phase was some form of $Fe_2(Si_x,Ti_{2-x})_2O_6$, possibly with additional Ti substituting for Fe (see discussion below).

Reconstructing the pre-exsolution garnet compositions

Several hundred spot analyses on the first generation garnets in samples 123220, 159966 and 540521b define compositional fields that are distinct from the garnet analyses from nearly forty other samples within the NSSZ that we have analyzed over the years (Fig. 6). These three samples define fields that are consistently lower in Al, at a given Si, and fall parallel to, and overlap with, the trend defined for majoritic garnets that have been analyzed from experimental studies and field samples (Haggerty and Sautter, 1990; Sautter et al., 1991; Ono, 1998). For 123220 and 159966, remixing the inferred exsolved Opx composition (TABLE 1) with the composition of the garnet mantle zones results in majorite-like compositions that are consistent with pressures of ~7.5 to 8.0 GPa (Table 1; see discussion below regarding P-T conditions).

Reconstructing the garnet composition for sample 540521b is complicated by the unusual composition of the exsolved phase. We hypothesize that the following multi-step recrystallization sequence is required to explain the observed phase relationships in these garnets:

Always consult and cite the final, published document. See http://www.minsocam.org or GeoscienceWorld

1. Exsolution of Fe- and Ti-rich Opx needles from a majoritic garnet
2. Recrystallization of the Opx needles to segmented rods, thermodynamically driven by surface energy minimization
3. Decomposition of the segmented rods to Qtz + Ilm.

Although this sequence is consistent with the textural requirements dictated by the phase morphologies, the stoichiometry of the reactant Opx cannot be reconciled with the Qtz + Ilm product assemblage, since the reactant Opx generally would have insufficient TiO_2 to generate the product assemblage. This problem may be resolved either through a coupled substitution of Ti + vacancy for 2 Fe in the M1 and M2 sites in the exsolved Opx, or through reaction of the exsolved opx with TiO_2 dissolved in the Grt but which was no longer thermodynamically stable in that cubic silicate structure. The former postulate is consistent with the observations in these samples of exsolved rutile (Rt) needles in Opx (discussed below), while the latter is consistent with observed Rt and Ilm lamellae in garnets in 123220 and 159966. Regardless of which mechanism is responsible for the observed phase relationships, a precursor majorite phase is necessary to account for the exsolution of Opx.

Diamond

Samples 123220 and 159966 have micron-scale carbon inclusions that occur within the inclusion-rich mantles of porphyroblastic garnets. These inclusions are optically flat in reflected light, without any indication of pleochroism, in contrast to

This is a preprint, the final version is subject to change, of the American Mineralogist (MSA)
Cite as Authors (Year) Title. American Mineralogist, in press.
(DOI will not work until issue is live.) DOI: http://dx.doi.org/10.2138/am.2014.4726

bladed graphite crystals that are a common accessory mineral phase in rocks of the supracrustal belts. These inclusions have a distinctive morphology (Fig. 7), only occur in the mantle zones of garnets, and consistently have cubic symmetry and faceted, pyramidal forms.

Raman spectra were collected on several of these grains (Fig. 8) in garnets from both samples. The grains in both samples consistently had well defined graphite modes (G and D peaks at primary wave numbers of ~1580 cm^{-1} and ~1355 cm^{-1}, respectively; Smith and Goddard, 2103). Also noted was a graphene (i.e., single graphite layer) peak at ~1420 cm^{-1} in some samples (Tiwari et al., 2012). In sample 123220 unambiguous peaks were also observed at 1335 cm^{-1}, which is the characteristic spectral peak for diamond. However, the diamond peak was not seen in all C inclusions in this sample, nor throughout a single inclusion. For example, for the larger inclusion (Figs. 7 & 8), "grain 5 large" two Raman spectra were collected in adjacent locations, one near the edge and one in the interior of the grain. The latter exhibited a well-defined diamond peak at 1335 cm^{-1} while the former did not. The presence of this characteristic peak unequivocally indicates the presence of crystalline diamond, since there are no other phases that share that mode.

To assure we were not detecting contamination from polish media, numerous other Raman spectra were collected in other types of inclusions, along grain boundaries and in late-stage graphite-hematite-magnetite veins. No peaks were observed at the characteristic diamond spectral location. In addition, the sample was re-polished using C-free polish media, in order to excavate the carbon inclusions to determine their 3-D

Always consult and cite the final, published document. See http://www.minsocam.org or GeoscienceWorld

This is a preprint, the final version is subject to change, of the American Mineralogist (MSA)
Cite as Authors (Year) Title. American Mineralogist, in press.
(DOI will not work until issue is live.) DOI: http://dx.doi.org/10.2138/am.2014.4726

morphology. Since platy forms would be expected for primary graphite blades, while cubic symmetry would be expected for primary diamond grains, distinguishing between these original forms allows determination of the original carbon crystallography (Chopin, 2003). The images obtained of these "cleaned" inclusions show them to be non-platy, cubic forms with faceted edges (Fig. 7), consistent with the entrapment of primary diamond during majorite growth. Raman spectra obtained on these "cleaned" inclusions revealed only nano-crystalline graphite, consistent with the interpretation that diamond was replaced by graphite that nucleated, at least in part, along the diamond-garnet interface.

We conclude from these observations that micro-diamond inclusions were present in first generation garnets in samples 123220 and 159966 and that they were encapsulated in the garnet during the growth stage at which the mantle zone developed. Later, during decompression and granulite facies metamorphism, diamond micro-inclusions were recrystallized to graphite, in a process similar to that recorded by Davies et al., (1993) and Smith and Godard (2013) for graphitized diamonds in the Ronda peridotite and the Norwegian Western Gneiss Region, respectively. Graphitization went to completion in sample 159966 but left relict micro-diamond grains during incomplete graphitization in sample 123220.

Rutile exsolution in garnet

Always consult and cite the final, published document. See http://www.minsocam.org or GeoscienceWorld

Commonly reported in UHP terrains are exsolution lamellae of rutile in garnets, pyroxenes and other phases. Although the origin of such needles has been the subject of debate (see discussion in Ague and Eckert, 2012) lamellae that occur in trigonal, interpenetrating orientation can only be derived through exsolution, and not epitaxial growth.

We have observed Rt exsolution lamellae (Fig. 9) in the core regions of the large (>5 cm diameter) euhedral garnet (sample 540599), which was collected from garnet-biotite-graphite-sillimanite schists within a few hundred meters of the site where sample 540521b was collected. The Rt needles are ca. a few hundred nanometers thick and tens to several hundreds of microns long. These needles have anomalous extinction angles of up to several tens of degrees. They are always oriented with inter-penetrating angles of close to 120^{o}, consistent with crystallographically controlled exsolution along <111>, as described by various researchers for needles exsolved from garnets in UHP terrains elsewhere (e.g., Larsen et al., 1998; Zhang and Liou 1999; Ye et al., 2000; Mposkos and Kostopoulos 2001; Zhang et al., 2003; Barron et al., 2005; Griffin et al., 1971; Griffin, 2008).

The mantle zones and exterior regions of such garnets commonly have inclusion trains of sillimanite, graphite, and feldspars, but these assemblages always occur exterior to the regions of the garnets with the Rt exsolution lamellae. The Rt lamellae are not observed associated with sillimanite or graphite. The garnet composition in the vicinity of the needles is $Py_{28}Sp_{2}Gr_{6}Al_{63}$. X-ray maps generated in the vicinity of the needles did not

This is a preprint, the final version is subject to change, of the American Mineralogist (MSA)
Cite as Authors (Year) Title. American Mineralogist, in press.
(DOI will not work until issue is live.) DOI: http://dx.doi.org/10.2138/am.2014.4726

385 reveal evidence of compositional variation in the immediate vicinity of the needles,
386 unlike those reported by Ague and Eckert (2012). We attribute this lack of zoning to re-
387 equilibration through diffusional processes controlled by compositional gradients during
388 granulite facies metamorphism post-dating the period of exsolution.
389
390 **Pyroxenes**
391
392 Pyroxene textures in the three samples of interest are complex and diverse. Each
393 sample possesses a different suite of compositional characteristics, but together they
394 provide a record consistent with recrystallization during recovery from UHP conditions.
395 Because of their diversity and complexity, the textures of each sample will be detailed
396 separately. We present them in order of increasing complexity. Their respective
397 compositions are presented in Ca-Mg-Fe ternary diagrams in Figure 10. The
398 nomenclature that we used is that of Morimoto et al. (1988).
399
400 *159966*
401 Opx and Cpx, along with Fa and Qtz, make-up the bulk of sample 159966. They
402 occur as approximately equant, anhedral millimeter-sized grains. The Cpx and Opx are
403 Mn- and Fe-rich Hd and Aug, and Fe-rich Fs, respectively. Mn content is 11%-12% of
404 the octahedral cations in the Fs and 5%-6% in the Cpx.
405
406 Although contacts between the pyroxenes are usually irregular and slightly lobate,
407 we also observed co-planar relationships in which Opx and Cpx shared in common (100)

Always consult and cite the final, published document. See http://www.minsocam.org or GeoscienceWorld

and (001) planes (Fig. 11a). The maximum a ^ c angle is 122°, based on measurements on Opx-Cpx pairs oriented with (010) in the plane of the thin section (Fig. 11a). This co-planar relationship suggests these may have been a single phase that unmixed during ascent from more severe P-T conditions. As discussed below, sample 540521b also contains evidence of unmixing of a coarse, homogeneous pyroxene phase.

The Cpx consistently exhibit three sets of exsolution lamellae. One set of lamellae consists of sharp-edged, tabular Opx (Fs) oriented parallel to (100) of the host Cpx (OpxL1 in Fig. 11b,c). These lamellae have associated with them very thin, sub-micron bands oriented within a few degrees of the (001) plane, and which terminate on either side of the Opx at small, round grains, resulting in a "dumbbell" morphology (red boxes in Fig. 11c). These features are consistently calcite (Cc). We interpret these OpxL1 to have been Pgt that initially exsolved from the Cpx during cooling and uplift, and later inverted to Fs and Cc. The Cc bands occupy the volume that formed in the inverted phase as a result of the volume change upon inversion.

Another set of lamellae occurs as small to large blebby forms that have strong preferred orientations in both the (100) and (001) planes of the host Cpx (OpxL2 in Fig. 11b). The third set of lamellae are very thin (ca. 1 micron) and wispy, and are inclined to the (100) plane by 3° to 6° (OpxL3 in Fig. 11c). These angular relationships are very close to those described by Robinson et al. (1971) for exsolution relationships involving Cpx-Opx-Pgt. We interpret OpxL3 to be exsolved Pig, based on similarities to the "fine

This is a preprint, the final version is subject to change, of the American Mineralogist (MSA)
Cite as Authors (Year) Title. American Mineralogist, in press.
(DOI will not work until issue is live.) DOI: http://dx.doi.org/10.2138/am.2014.4726

pigeonite lamallae, which orient in acute angle ß of host augite" reported by Ollila et al (1988).

Opx contain barely discernible Cpx lamellae and prominent Mag and Ilm lamellae oriented parallel to (100) (Fig. 11b,d). The oxide phases often coexist in the same lamella and appear to have unmixed.

123220

The bulk mineralogy of 123220 is identical to that of sample 159966, except that Pgt porphyroblasts are also present as elongate, 1-10 mm-size grains that define a fabric in restricted portions of the sample. As with sample 159966, elongate garnet porphyroblasts also occur and are elongate parallel to the fabric defined by the Pig.

The Pgt porphyroblasts consistently have aligned inclusions parallel to the {001} zone that are composed of Fa – Qtz – Fe-rich Aug (Fig. 12a,c). The relative proportions of these three phases vary within narrow ranges among the inclusions. A few of the inclusions have unequivocal idiomorphic forms (Fig. 12a,c) consistent with Opx. On the basis of these observations, we interpret these inclusions to be exsolved Fs that inverted to the three-phase assemblage Fa + Fe-rich Aug + Qtz. We have no quantitative determination of the relative proportions of the phases, but a reaction consistent with this surmise, and which honors the relative observed volumetric proportions (Ol : Qtz : Cpx ~ 1 : 1 : 0.25) is (phase compositions based on remixed probe compositions of the reactant phases):

Always consult and cite the final, published document. See http://www.minsocam.org or GeoscienceWorld

453

454 $(Ca_{0.16}Mg_{0.06}Fe_{1.56}Mn_{0.22})_{2.0}(Al_{0.006}Si_{1.994})_{2.0}O_6$

455 (Fs)

456 ⇔

457 $0.8\ (Mg_{0.04}Fe_{1.72}Mn_{0.24})_{2.0}SiO_4$

458 (Fa)

459 +

460 $0.202\ (Ca_{0.79}Mg_{0.12}Fe_{0.93}Mn_{0.14})_{2.0}(Al_{0.03}Si_{1.97})_{2.0}O_6$

461 (Fe-rich Aug)

462 +

463 $0.796\ SiO_2$

464 (Qtz).

465

466 Additionally, the Pgt grains consistently have Rt exsolution lamellae that are
467 aligned parallel to each other and lying within the plane of the dominant cleavage (Fig.
468 12b).

469

470 Fe-rich Aug that is a reaction product of the breakdown of Fs, as well as
471 individual Cpx grains in the rock matrix also consistently contain Opx exsolution
472 lamellae that are indistinguishable from the OpxL1 lamellae in 159966 (Fig. 12d). In
473 addition, cuspate grain boundaries between Fa and exsolved Opx that are aligned with
474 exsolution features (Fig. 12d) are consistent with the model that exsolution and
475 recrystallization of the bulk rock, to some extent, were coeval. These features are very

This is a preprint, the final version is subject to change, of the American Mineralogist (MSA)
Cite as Authors (Year) Title. American Mineralogist, in press.
(DOI will not work until issue is live.) DOI: http://dx.doi.org/10.2138/am.2014.4726

similar to those reported by Holness et al. (2011) for late-stage crystallization processes in the Skaergaard intrusive complex.

The compositions of these phases are more Fe-rich than those in sample 159966 and 540521b (discussed below) (Fig. 10). Even so, the very close compositional similarity of these minerals to those in sample 159966 suggest that they are likely to be samples from lithologic units with identical precursor protoliths. The unequivocal Pgt compositions preserved in this sample are relatively rare within the metamorphic literature, and attest to temperatures in excess of 825^{o}C (Lindsley, 1983; Harley, 1987; Hyslop et al., 2008).

540521b

The bulk mineralogy of 540521b is unusual. The bulk rock consists predominantly of Opx- and Cpx, with equant Grt porphyroblasts. Minor amounts of Mag, Rt, Gr, Mnz and carbonate are also present. The pyroxenes exhibit multiple exsolution features that complexly relate to each other.

The most obvious exsolution lamellae are coarse Fe-rich Hd (CpxL-1) that are 10-50 microns wide and up to 1 cm long (Fig. 13a,b,c). They are rod-shaped, with undulous grain boundaries and rounded terminations, thus giving the appearance they have undergone some degree of recrystallization after originally exsolving from an earlier host. These lamellae occur in Opx (Opx2), and form distinct sets in which members of each set parallel each other and are approximately regularly spaced. They are observed to crosscut

Always consult and cite the final, published document. See http://www.minsocam.org or GeoscienceWorld

This is a preprint, the final version is subject to change, of the American Mineralogist (MSA)
Cite as Authors (Year) Title. American Mineralogist, in press.
(DOI will not work until issue is live.) DOI: http://dx.doi.org/10.2138/am.2014.4726

499 other Opx exsolution features and cleavage, and occasionally lay along grain boundaries
500 between separate Opx grains. As such, they bear no systematic relationship to the
501 present-day Opx grain structure. However, based on their textural form and overall
502 characteristics, we interpret them to be Cpx exsolution lamellae from an earlier pyroxene,
503 analogous to similar Cpx exsolution from pyroxenes in the Nain Anorthosite complex
504 (Smith, 1974), Enderby Land (Harley, 1987) and the Skaergaard Intrusion (Holness et al.,
505 2011). The ternary compositions of these lamellae are plotted as the blue star in Figure 10.
506
507 Individual host Opx grains (Opx2) also contain a younger generation (based on
508 cross-cutting relationships) of well-developed, linear, sharp-edged Cpx exsolution
509 lamellae (CpxL-2; Fig. 13b,c) parallel to (100). These lamellae cluster near the Hd - high-
510 Ca Aug (Fig. 10) range, and possess sub-micron Opx exsolution lamellae that are nearly
511 perpendicular to the long-axis of the host Cpx lamellae. Based on similarity of form and
512 relative chronology, we infer these Cpx-hosted Opx lamellae to be equivalent to the Opx
513 lamellae in 123220 (Fig. 12d).
514
515 The bulk rock clinopyroxene grains have two distinct sets of exsolution lamellae,
516 similar in morphology and orientation to OpxL1 and OpxL3 observed in sample 159966.
517 We infer them to be of the same relative chronology and significance.
518
519 Also observed in Opx2 are rare omphacite (Omp) + Cc lamellae. These occur as
520 well-defined lamellar structures (Fig. 13b) or as blebs at the terminations of Cpx lamellae
521 in Opx. The Omp composition was consistently within a few percent of

Always consult and cite the final, published document. See http://www.minsocam.org or GeoscienceWorld

This is a preprint, the final version is subject to change, of the American Mineralogist (MSA)
Cite as Authors (Year) Title. American Mineralogist, in press.
(DOI will not work until issue is live.) DOI: http://dx.doi.org/10.2138/am.2014.4726

522

523 $(Na_{0.13}Ca_{0.44}Mg_{0.12}Fe_{0.31})_{1.00}(Mg_{0.19}Fe^{2+}_{0.51}Mn_{0.04}Al_{0.29}Ti_{0.02})_{1.03}(Al_{0.23}Si_{1.77})_{2.0}O_6$.

524

525 This composition is unusual in that the stoichiometry appears to require a
526 substantial proportion of Mg and Fe^{2+} in the M2 site. In terms of the ternary components
527 acmite-jadeite-(diopside-hedenbergite-CaTschermakite) this Omp are sodian augite
528 (Essene and Fyfe, 1967) which are associated with type A eclogites. We interpret these
529 Na- and Al-rich pyroxenes, and the Cc with which they are always associated, to be
530 exsolved phases from the Cpx exsolution lamellae.

531

532 The sets of coarse CpxL-1 lamellae that are discordant to later generations of
533 pyroxene lamellae and grain boundaries, must represent the remnants of an earlier
534 mineralogy. We have reconstructed the textural relationships of that mineralogy by
535 assuming that coherent sets of lamellae formed from the same grain. On this basis we re-
536 constructed the pre-existing grain boundaries, assuming that the areal limit of each
537 coherent set approximated the extent of the original grain (Fig. 14). The results show that
538 the earlier grains were significantly coarser (> 0.3 cm) than the current host pyroxene
539 grains, and they appeared to form a polygonal mosaic, rather than the irregular grain
540 geometries exhibited by the current bulk rock pyroxenes.

541

542 **Olivines and Ahrensite (Fe-Ringwoodite) (?)**

543

Always consult and cite the final, published document. See http://www.minsocam.org or GeoscienceWorld

This is a preprint, the final version is subject to change, of the American Mineralogist (MSA)
Cite as Authors (Year) Title. American Mineralogist, in press.
(DOI will not work until issue is live.) DOI: http://dx.doi.org/10.2138/am.2014.4726

In sample 123220, three discrete generations of olivines occur. The oldest olivines (Ol-1) occur as rounded inclusions in the mantle zones of first generation garnets. These olivines are the most Mg-rich (~ $Fo_{3.75}Fa_{85}Tep_{11.25}$) of any observed in sample 123220 (Fig. 15). Olivine suite Ol-2 are the poorest in Mg (~ $Fo_{1.8}Fa_{86}Tep_{12.2}$), and only occur within inclusions in Pgt. These Ol-2 olivines are the reaction products from the breakdown of Fs to Fa + Fe-Hd + Qtz. Olivine suite Ol-3 (~ $Fo_{2}Fa_{86}Tep_{12}$) compose the bulk of the olivines in this rock, and consistently are in contact with quartz. These groundmass olivines occasionally have sets of lamellae of Mag and Fs.

Olivines in sample 159966 appear, optically, to be of a single generation, and are invariably in contact with quartz. They, too, have individual lamellae of Mag. The compositional range of olivines from both samples span the same range, although there is a clear clustering at higher Mg values for the olivines in sample 159966.

An unusual feature observed in sample 123220 are very fine Qtz lamellae in the core of a few Fa grains (Fig. 16a,b). These lamellae occur in small clusters and commonly terminate along prominent cracks. The compositions of the hosting fayalitic olivines was $Fo_2Fa_{86}Tep_{12}$, which overlaps with that of the olivines in the bulk rock. The morphology of these Qtz lamellae are reminiscent of exsolution features. In addition, the lamellae have a consistent crystallographic orientation with respect to each other and the enclosing olivine. These characteristics strongly suggest that the Qtz lamellae exsolved from the enclosing grains. We speculate that these lamellae are evidence for the earlier presence of ahrensite (i.e., Fe-ringwoodite), as detailed in the Discussion section, below.

Always consult and cite the final, published document. See http://www.minsocam.org or GeoscienceWorld

DISCUSSION

The presence of remnant diamonds in graphitic inclusions in garnet mantles in sample 123220, and similar graphitic inclusions in sample 159966, establishes that at least portions of the supracrustal belts close to the northern boundary of the NSSZ must have experienced P-T conditions associated with UHP metamorphism.

The presence of inclusions that, although recrystallized to Cl-bearing hydrous phases, have integrated bulk compositions of Opx, and for which crystallographic orientations are consistent with exsolution from garnet, provide strong evidence that the garnets crystallized as majorite during the period of time at which the mantle regions of the garnets in 123220 and 159966 grew. This is strong corroborating evidence that these rocks experienced P-T conditions well within the UHP metamorphic regime. Phase assemblages and compositions provide additional corroborating evidence through thermobarometric models and phase equilibria calculations.

P-T Constraints From Geothermometry, Geobarometry and Phase Equilibria

A number of calibrations have been published for calculating temperatures from co-existing Opx and Cpx, and pressures from coexisting Opx-Grt. Both assemblages are common in these samples. We have chosen to use the calibration of Brey and Kohler (1990) because it was dderived from fits to high pressure experimental data and provides

This is a preprint, the final version is subject to change, of the American Mineralogist (MSA)
Cite as Authors (Year) Title. American Mineralogist, in press.
(DOI will not work until issue is live.) DOI: http://dx.doi.org/10.2138/am.2014.4726

590 the most consistent results for our samples, while also corresponding to constraints
591 derived from phase equilibria and Thermocalc (v3.36; Holland and Powell, 2011)
592 models (described below) for these rocks. However, the unusual composition of the rocks
593 we describe in this study does not directly correspond to any experimental systems
594 relevant for UHP studies. In particular, the Mn-rich nature of the phases is associated
595 with important non-ideal thermodynamic properties (e.g., Geiger and Feenstra, 1997).
596 The P-T conditions computed for these rocks, therefore, are subject to uncertainties that
597 cannot be quantified at this time and the P-T conditions that we present must be
598 considered tentative. In addition, the complex exsolution and recrystallization histories
599 recorded by these rocks require careful assessment of textural relationships to determine
600 the appropriate EMP-derived compositions to use for calculating a P and T for a
601 particular stage in the recrystallization history of these rocks.
602
603 The appropriate compositions to use for calculating P-T conditions for the
604 inversion of majorite to Grt + Opx are the re-mixed garnet + 6% Opx compositions
605 (Table 1) and the computed Opx composition from the reconstituted alteration products
606 (Table 1) studied in detail for sample 159966. We applied the same strategy to 123220,
607 assuming the exsolved orthopyroxene had the same composition as that in 159966.
608 Although this will introduce some error in the calculation, the nearly identical
609 compositions of all phases in these two rocks make such an approach reasonable, and the
610 resulting error likely to be very minor. We also computed the re-mixed Opx and Cpx in
611 the bulk rock, and computed temperature as a function of pressure. The intersections of
612 the trajectories of P-T points for these Grt-Opx and Opx-Cpx calibrations allows P and T

Always consult and cite the final, published document. See http://www.minsocam.org or GeoscienceWorld

This is a preprint, the final version is subject to change, of the American Mineralogist (MSA)
Cite as Authors (Year) Title. American Mineralogist, in press.
(DOI will not work until issue is live.) DOI: http://dx.doi.org/10.2138/am.2014.4726

to be established at time of the majorite-garnet transition. These intersections should occur near the lower pressure limit for majorite stability.

The resulting P and T are essentially identical for the two samples; 7.0 (+/- 1.0) GPa, 975 (+/- 55)^{o}C for 123220 and 6.9 (+/- 1.0) GPa, 985 (+/- 60)^{o}C for 159966 (Fig. 17). These intersections fall just below the lower pressure limit for the majoritic garnets of this composition, and closely correlate to conditions inferred from the mixing lines of Sautter et al (1991) (Figs. 6 and 17). The consistency of these independent approaches lends credence to the validity of these results. Even so, the strong disparity between the compositions of these phases and the experimental systems upon which the calculations are based requires that these results be viewed with caution.

Temperatures for sample 540521b were computed using the integrated compositions for the coarse Opx and Cpx. Pressure was computed using the range of garnet compositions in the mantle zones in which exsolution lamellae of Fs + Rt (inferred) was observed. We did not re-integrate the garnet compositions because of the unusual Fe-Ti characteristics of that system. The computed P and T were 8.0 (+/- 0.8) GPa and 1051 (+/- 80)^{o}C, respectively. Our experience with samples 123220 and 159966 showed that re-integrating the garnet-orthopyroxene compositions lowered the pressures by about 1 GPa, (compared to un-reintegrated compositions) which we also believe would be the case if the garnet compositions of 540521b could have been re-integrated for this sample.

Always consult and cite the final, published document. See http://www.minsocam.org or GeoscienceWorld

This is a preprint, the final version is subject to change, of the American Mineralogist (MSA)
Cite as Authors (Year) Title. American Mineralogist, in press.
(DOI will not work until issue is live.) DOI: http://dx.doi.org/10.2138/am.2014.4726

We also computed the pressure-dependent Opx-Cpx temperatures for various observed compositional combinations of Cpx lamellae and Opx host, and Opx lamellae and cCpxpx hosts (dashed lines in Fig. 17). In all cases, these un-mixed compositions provide temperatures that are incompatible with constraining phase equilibria (e.g., Fs ⇔ Fa + Qtz; and Cpx-Opx-Pgt; see discussion below). We conclude that these compositions represent diffusional re-equilibration of the thin Cpx-Opx lamellae pairs during cooling and uplift.

Constraining Phase equilibria

Three phase relationships provide tight P-T constraints on the evolution of these rocks, beyond those provided by the diamond and majorite assemblages. These constraints are based on computed P-T conditions using Thermocalc (v3.36, ds61; Holland and Powell, 2011) for reactions Fs ⇔ Fa + Qtz and Fs + Rt ⇔ Ilm + Qtz; and experimental results that establish conditions for the coexistence of the 3-phase pyroxene assemblage Cpx-Opx-Pgt for the compositions we observe (Lindsley, 1983).

Sample 123220 provides unequivocal evidence of the reaction

$$\text{Fs} \Leftrightarrow \text{Fa} + \text{Qtz} (+ \text{Cpx})$$

as inclusions in Pgt (Fig. 12). The reactant assemblage is also the common bulk-rock mineralogy of this sample, which requires that at least part of the present day Fa-Qtz assemblage that is dominant in this rock must be derivative from inversion from an

Always consult and cite the final, published document. See http://www.minsocam.org or GeoscienceWorld

This is a preprint, the final version is subject to change, of the American Mineralogist (MSA)
Cite as Authors (Year) Title. American Mineralogist, in press.
(DOI will not work until issue is live.) DOI: http://dx.doi.org/10.2138/am.2014.4726

earlier Fs-dominated paragenesis. For the compositions of the reaction products, the conditions of formation are enclosed within the small shaded ellipse in Figure 17, i.e., 0.9 GPa at 885°C to 1.7 GPa at 960°C. The P-T trajectory of sample 123220 must pass through this region upon decompression and cooling. Given the ubiquitous presence in the rock matrix of this reactant assemblage in sample 159966, and the near-identical composition of the mineral phases to those in sample 123220, sample 159966 must also have followed the same P-T trajectory through this set of conditions.

The coexistence of the 3-phase pyroxene assemblage Cpx-Opx-Pgt in sample 123220 also constrains P-T conditions, since this unusual assemblage will persist in a narrow P-T band, for the phase compositions observed in this sample. Based on the experimental data of Lindsley (1983), the linear trajectory from the high P-T conditions recorded by the exsolved Opx in garnets in this sample, to the Fa + Qtz field, crosses the 3-pyroxene field at 2.9 (+/- 0.2) GPa at 950 (+/- 15)°C (Fig. 17).

The assemblage of Ilm + Qtz is contained in the segmented remnants of exsolved rods in the garnets in sample 540521b. The reaction

$$Fs + 2\ Rt \Leftrightarrow 2\ Qtz + 2\ Ilm$$

constrains the the P-T conditions for the development of this assemblage since the product-side of this reaction, which is the high T – low P assemblage, is now the defining mineralogy of the rods. We used Thermocalc to compute the conditions for this reaction

Always consult and cite the final, published document. See http://www.minsocam.org or GeoscienceWorld

This is a preprint, the final version is subject to change, of the American Mineralogist (MSA)
Cite as Authors (Year) Title. American Mineralogist, in press.
(DOI will not work until issue is live.) DOI: http://dx.doi.org/10.2138/am.2014.4726

682 (Fig. 17). Since sample 540521b was collected approximately 2 km east of sample
683 123220, the uplift trajectory of these two samples is likely to be very similar, thus
684 suggesting that the Ilm + Qtz assemblage developed during decompression at
685 approximately 4 GPa at 980°C. We note, however, that the extremely small size of the
686 individual grains may result in some surface energy contribution to the overall energetics
687 of the reaction, and hence may bias, to some unknown extent, the actual P-T of the
688 reaction to conditions that are different from those calculated.
689
690 Pyroxene textures, particularly in samples 159966 and 540521b, indicate that
691 these garnet pyroxenites were composed of a single pyroxene phase (coarse-grained Fe-
692 rich Aug or Fs) that coexisted with majoritic garnet. The enrichment in light rare earth
693 elements observed in the garnet mantles is consistent with the solubility of a pyroxene
694 component in garnet (i.e., majorite), since pyroxenes consistently have higher La/Yb
695 ratios than garnets (Mazzucchelli et al., 1992; Vannucci et al., 1994). Hence, these rocks,
696 at their most extreme UHP conditions, were majorite pyroxenites. In the case of sample
697 123220, ahrensite may have been present with this assemblage.
698
699 This sequence of exsolution and phase re-equilibration suggests that
700 decompression was almost isothermal, with a ΔT of 100°C to 150°C over a ΔP of about 6
701 GPa. During this decompression, Rt needles exsolved from garnets and Omp + Cc
702 exsolved from pyroxenes. Although Rt exsolving from garnets is clearly associated with
703 UHP metamorphism (Ague and Eckert, 2012), and Omp is a common pyroxene in high-
704 pressure eclogites (Coleman et al., 1965; Ernst and Liou, 2008), their presence can only

Always consult and cite the final, published document. See http://www.minsocam.org or GeoscienceWorld

This is a preprint, the final version is subject to change, of the American Mineralogist (MSA)
Cite as Authors (Year) Title. American Mineralogist, in press.
(DOI will not work until issue is live.) DOI: http://dx.doi.org/10.2138/am.2014.4726

be used to confirm the UHP history of these rocks, but cannot be used to specify specific P-T conditions because their development can occur over a very wide P-T range.

Are the quartz lamellae in fayalite evidence for prior ahrensite?

As previously noted, Qtz needles with the textural characteristics of exsolution lamellae occur in a few rare olivines in sample 123220. Since these olivines are currently stoichiometric Fa, the presence of lamellae of Qtz requires that a prior phase accommodated excess silica. To our knowledge, exsolution of Qtz from olivine has not been reported in the literature, nor have there been reports of super-silicic olivine. However, Akaogi and Akimoto (1979), Irifune and Ringwood (1987) and Hazen et al. (1993), have shown that the UHP wadsleyite-ringwoodite (i.e., spinel-structured olivine) series can contain excess Si. Theoretically, therefore, spinel-structured olivines in the wadsleyite-ringwoodite series would exsolve silica upon decompression and inversion to olivine if they were initially super-silicic. We therefore speculate that the Qtz needles observed in our sample might have developed in response to inversion of high-pressure supersilicic ahrensite to Fa upon decompression. If this were the case, excess Si in the ahrensite would have to be accommodated via a vacancy substitution mechanism in which $\square SiFe_{-2}$ (Day and Mulcahy, 2007) occurs. Upon inversion of ahrensite to Fa during decompression, the reaction

$$(Fe_2SiO_4 + (Fe_2SiO_4 + \square SiFe_{-2})) \Leftrightarrow (Fe_2SiO_4 + (Fe_2SiO_4 + \square SiFe_{-2}))$$

ahrensite $\Leftrightarrow$ Fa with excess Si

Always consult and cite the final, published document. See http://www.minsocam.org or GeoscienceWorld

This is a preprint, the final version is subject to change, of the American Mineralogist (MSA)
Cite as Authors (Year) Title. American Mineralogist, in press.
(DOI will not work until issue is live.) DOI: http://dx.doi.org/10.2138/am.2014.4726

would result. This phase inversion would be followed (or accompanied) by exsolution of Qtz lamellae via the reaction

$$(Fe_2SiO_4 + (Fe_2SiO_4 + \square SiFe_{-2})) \Leftrightarrow Fe_2SiO_4 + 2\,SiO_2.$$

Fa with excess Si Fa Qtz

Although highly speculative, this explanation for the Qtz lamellae are consistent with exsolution lamellae of Ilm and chromite (Chr) in Ol, interpreted to have exsolved during inversion of UHP spinel-structured olivine to Ol, (Dobrzhinetskaya et al., 1996, 2000; Bozhilov, 2003). As we noted previously, Mag lamellae in the olivines also occur in 123220. These may be analogous to the Ilm and Chr lamellae reported previously, which would be consistent with the Fe-rich nature of this assemblages and the interpretation of the prior presence of ahrensite.

For the pure Fe-Mg system, the composition of the olivines observed in this sample would require that the pressure conditions for the initial inversion would be ca. 5 GPa at 1200°C. For lower temperatures, a lower pressure would be required, but the minimum P-T for ahrensite formation has not been established.

Defining the prograde metamorphic path

There are very few unequivocal remnants of minerals useful for defining the prograde metamorphic path of these rocks. One important observation that is useful for deducing the prograde path, however, is that the first mineral to form on the retrograde

Always consult and cite the final, published document. See http://www.minsocam.org or GeoscienceWorld

This is a preprint, the final version is subject to change, of the American Mineralogist (MSA)
Cite as Authors (Year) Title. American Mineralogist, in press.
(DOI will not work until issue is live.) DOI: http://dx.doi.org/10.2138/am.2014.4726

751 path these rocks experience is amphibole, which replaces pyroxenes in all rocks in
752 localities in the immediate vicinity (on the scale of meters) of the samples described in
753 this report. This fact suggests that amphibole is a likely precursor mineral phase in the
754 prograde development of the mineral assemblages of interest. Consistent with this
755 observation is the fact that the normalized REE pattern values for Eu through Dy in the
756 garnets in 123220 (Fig. 4) exactly parallel the variation pattern obtained by Konrad-
757 Schmolke et al (2008) in their forward modeling of Grt growth from amphibole (Amp)
758 breakdown. The convex-upward hump in this portion of the REE pattern results from
759 breakdown of Amp and a Cpx I to Grt and a Cpx II. Their modeling also results in an
760 enrichment in the Ca-component in the Grt, which we also observed in the inner to
761 middle mantle zone in 123220 (Fig.4d).
762
763 Assuming that an Amp phase was part of earlier mineral assemblages,
764 Schmädicke and Evans (1997) calculated the locations of equilibria in ultramafic rocks
765 from Erzgebirge (Bohemian Massif) that, among other relationships, defined garnet-
766 genesis reactions from amphibole-breakdown using an early version of Thermocalc
767 (Holland and Powell, 1990). The computed P-T constraints are indicated by the green
768 box in Figure 17. Konrad-Schmolke et al. (2008), calculated similar constraints for
769 eclogitic rocks from the Western Gneiss Region (Norway) using a separate forward-
770 calculation approach. Their results are shown as the blue box in Figure 17. We conducted
771 phase equilibria calculations using a more recent version of Thermocalc and the bulk
772 composition for sample 123220. The results of these calculations are the blue cross in

Always consult and cite the final, published document. See http://www.minsocam.org or GeoscienceWorld

This is a preprint, the final version is subject to change, of the American Mineralogist (MSA)
Cite as Authors (Year) Title. American Mineralogist, in press.
(DOI will not work until issue is live.) DOI: http://dx.doi.org/10.2138/am.2014.4726

773 Figure 17. All of these calculations define a broad but consistent field in P-T space
774 through which sample 123220 must have passed during subduction.
775
776 We conclude that the overlapping P-T conditions from these diverse studies, and
777 the compositional correspondences for REE and Ca, provide strong evidence that the
778 prograde path for sample 123220 must have been close to the P-T conditions indicated by
779 the blue cross in Figure 17.
780
781 The earliest portion of the prograde path is recorded by the Fe-rich, clear core
782 zones in the garnets where, in addition, striking enrichments in Ti and Cr were previously
783 noted. Given the high concentrations of Fe and Mn in these rocks, we speculate that the
784 initial low- to medium grade metamorphic assemblages in these rocks may have
785 contained a piemontite-like phase along with Mag/maghemite/Ilm phases. If that were the
786 case, the initial and lowest grade garnet-forming reactions may well have involved these
787 minerals, which likely would have partitioned minor and trace components such as Cr
788 and Ti into the Grt reaction products.
789
790 *Regional variations and location of the subduction complex*
791
792 Figure 17 compares the maximum P-T conditions of these UHP samples with a
793 selected suite of other trajectories deduced from other samples in the NSSZ. Sample
794 492042E is an HP Grt-Spl-Ol gneiss (Glassley et al., 2007) that is from a similarly
795 positioned supracrustal unit as the samples described here, but occurring more than 25

Always consult and cite the final, published document. See http://www.minsocam.org or GeoscienceWorld

This is a preprint, the final version is subject to change, of the American Mineralogist (MSA)
Cite as Authors (Year) Title. American Mineralogist, in press.
(DOI will not work until issue is live.) DOI: http://dx.doi.org/10.2138/am.2014.4726

796 km to the east of 159966 (see Fig. 1). Its decompression trajectory is very similar to that
797 of the UHP samples. The other trajectories are from different rock units that are 15 km to
798 the southeast (Marranguit, a sequence of marbles and pelitic schists) and >30 km east
799 (468340 and 492045, mafic gneisses) of the UHP sample sites. The contrasting P-T
800 trajectories recorded by the UHP and HP samples, relative to all other well-constrained
801 trajectories in the NO, suggest that a high degree of tectonic interleaving is required to
802 juxtapose rocks with such different pressure histories. Whether this reflects complex
803 mixing processes within a subduction channel, tectonic imbrication during continent-
804 continent collision or tectonic slicing during development of the shear zone, or all three,
805 remains a question for further investigation.
806
807 These UHP conditions greatly exceed those that have long been inferred for any
808 part of the Paleoproterozoic rocks of West Greenland (e.g., Hansen, 1979; Glassley and
809 Sørensen, 1980; van Gool et al, 2002), which has experienced a well-documented upper
810 amphibolite to granulite facies metamorphism at ca. 1850 my (Hickman and Glassley,
811 1984; Taylor and Kalsbeek, 1990; Kalsbeek and Nutman, 1996; Connelly and Mengel,
812 2000; Connelly et al., 2000). We attribute this late discovery of the UHP metamorphic
813 episode to several factors. First, although two (123220 and 159966) of the four samples
814 we describe here were collected in the late 1960s and early 1970s, the significance of
815 their mineralogy could not have been established at that time because there was very little
816 experimental data that would have suggested such high pressure conditions were
817 recorded in those rocks. Second, the vast majority of rocks in this terrain have been
818 through pervasive deformation and recrystallization under typical upper amphibolite to

Always consult and cite the final, published document. See http://www.minsocam.org or GeoscienceWorld

819 granulite facies conditions. This deformation has been associated with influx of fluids
820 and metasomatic alteration and recrystallization (Glassley et al., 2010). Preservation of
821 UHP mineralogy is exceedingly rare, as a result, and confined to those volumetrically
822 trivial rock masses that have escaped elevated H_2O activity/infiltration and deformation.
823 The consistent presence of Cc with exsolved Omp, and with inverted pyroxenes may
824 imply that elevated CO_2 activity prevented thorough hydration/recrystallization of these
825 rocks by buffering them to low a_{H2O}. Third, the unusual bulk rock composition (Fe- and
826 Mn-rich; alkali-, Mg-, Al- and Si-poor) of these samples favors development of
827 characteristic UHP mineralogies (e.g., majoritic garnets; complex pyroxene relationships,
828 etc.) at the lowest P-T range reached by these mineral assemblages. Bulk rock
829 compositions that are Mg-richer and Fe-poorer require significantly higher P-T
830 conditions for the characteristic mineralogical features to develop.
831
832 These UHP samples resolve uncertainty that has persisted regarding the location
833 of a "cryptic" suture in this region (Kalsbeek et al., 1987; van Gool et al., 2002; Glassley
834 et al., 2010). Given that UHP conditions result from processes within subduction
835 complexes, it is clear that the subduction zone that was active in this region must have
836 been located along the northern boundary of the NSSZ, and that late stage shearing that
837 so prominently deforms these rocks represents oblique shear of the subduction mélange
838 complex during and after continent-continent collision.
839
840 *Comparison with other UHP terrains*
841

842 Figure 18 shows that the NSSZ UHP samples fall at the high pressure – low
843 temperature range of previously reported UHP locations. Given that the previous reports
844 are from much younger terrains, this set of P-T conditions is somewhat surprising. What
845 this may mean for Paleoproterozoic mantle conditions in subduction zones remains
846 unclear until more such sites are identified and studied. Either subduction rates at this
847 location were rapid enough to cool the subduction zone, resulting in deeply suppressed
848 isotherms, or mantle thermal gradients were relatively low. It is evident, however, that
849 exhumation rates must have been exceedingly high in order for thermal conditions to
850 have changed such a small amount during uplift. Even so, the trajectory in P-T space
851 follows closely that depicted by Gilotti (2013) for "hot" UHP trajectories, except at the
852 very highest pressure region where our UHP samples marginally cross into the so called
853 "forbidden zone".
854
855 The interpretation we present that the delicate quartz needles preserved in olivine
856 in sample 123220 represent exsolution from a ringwoodite phase is speculative. Given
857 that the bulk of fayalite in this sample formed as a result of ferrosilite breakdown to
858 fayalite and quartz at pressures less than 2 GPa, our interpretation can be correct only if
859 the UHP assemblage was initially garnet – ringwoodite - Fe-rich augite/ferrosilite (+/-
860 fayalite). Upon decompression, ringwoodite would invert to olivine with excess silica
861 through a vacancy substitution scheme. At some point below the ferrosilite-breakdown
862 reaction to fayalite plus quartz (or perhaps during that process), exsolution of the quartz
863 needles occurred. The fact that the clusters of needles are commonly sharply terminated
864 at prominent cracks in the fayalite suggests that nucleation and growth of the quartz

This is a preprint, the final version is subject to change, of the American Mineralogist (MSA)
Cite as Authors (Year) Title. American Mineralogist, in press.
(DOI will not work until issue is live.) DOI: http://dx.doi.org/10.2138/am.2014.4726

lamellae may have been initiated along discrete zones stressed by crystallographic adjustments related to relaxation associated with the vacancy substitution scheme previously noted. However, further experimental work and recovery of similar samples that preserve the sequence of events we postulate is needed to evaluate this speculation.

IMPLICATIONS

Remnants of majoritic garnet, diamond, rutile needles exsolved from garnet and pyroxenes, and complex pyroxene exsolution textures that include exsolution of omphacite, along with possible evidence of ringwoodite, indicate that a previously unrecognized UHP metamorphic rock sequence exists in the western region of the Nagssugtoqidian shear zone near and along its northern boundary. This metamorphic complex formed during Paleoproterozoic subduction and marks the location of the suture that formed during continent-continent collision ca. 1850 mya. This is the first report of UHP metamorphism in the Paleoproterozoic rocks of West Greenland.

Although providing new insight into the complex tectonic history of this region, further work needs to be conducted to resolve the following key outstanding issues:

1. Are the UHP rocks contained within a tectonic slice transported from depth and interleaved into lower P-T rock units, or is there a continuous UHP terrain in this region?
2. The unusual composition of these rocks does not directly correspond to any experimental systems relevant for UHP studies. In particular, the Mn-rich nature

Always consult and cite the final, published document. See http://www.minsocam.org or GeoscienceWorld

of the phases is associated with important non-ideal thermodynamic properties (e.g., Geiger and Feenstra, 1997). The P-T conditions computed for these rocks, therefore, are subject to uncertainties that cannot be quantified at this time. Further experimental and theoretical work needs to be done that would allow these uncertainties to be quantitatively evaluated.

3. Is the unexpectedly low T at high P for these UHP rocks representative of mantle conditions during the Paleoproterozoic or are these rocks recording aberrant conditions relative to the average thermal structure in subduction zones of that period? Or, do these UHP rocks record very rapid subduction rates that may have been characteristic for Paleoproterozoic subduction systems?
4. The postulated presence of reaction products from ringwoodite breakdown is speculative. Further work needs to be done to test this suggestion. If it is correct, ringwoodite remnants may be present in other UHP regions in which Fe-rich assemblages occur.

The ability to identify these unusual assemblages reflects a serendipitous confluence of circumstances – Fe- and Mn-rich rocks that were relatively undeformed, and escaped significant hydration during exhumation. These observations suggest that such lithologies should be considered targets for detailed investigations in regions where HP or UHP conditions may be suspected.

Acknowledgements

Steen Platou joined us in the field in Greenland in July and August of 2012, more than forty years after his last field season, when he was there for his thesis work as a student at

This is a preprint, the final version is subject to change, of the American Mineralogist (MSA)
Cite as Authors (Year) Title. American Mineralogist, in press.
(DOI will not work until issue is live.) DOI: http://dx.doi.org/10.2138/am.2014.4726

Aarhus University. His thesis work was an integral part of the mapping campaign in the late 1960s and early 1970s that established the foundation for much of what we know about West Greenland Nagssugtoqidian geology. During that time, he established one of the first computer-oriented GIS systems, which was widely adapted for field work in West Greenland. We returned to the area he mapped, with him as field guide, to relocate one of the key samples for this work (123220), which he had collected so long ago. He was a stalwart field companion, with a wry sense of humor. When we speculated, he grounded us in skepticism; when we groused, he made us laugh. When we returned from the field, he continued with his passion of refining and digitizing field maps and documents. Suddenly, while involved in this compilation work, Steen died. We have lost a friend and colleague, but we acknowledge with thanks the good fortune we had of sharing with him a wilderness place he so dearly enjoyed.

We also would like to acknowledge the assistance of Andrew Fowler in collecting and reducing the LA-ICP-MS data; Alan Hicklin of the Keck Spectral Imaging Facility, Department of Chemistry, U.C. Davis for assistance with the Raman spectrometry; Isabel Montanez for assistance with and use of the 3-D imaging; and Sarah Roeske and Nick Botto for their boundless support on the electron microprobe. Comments on various parts of this paper by Howard Day and Robert Zierenberg are gratefully acknowledged.

Thorough, critical reviews by W.L. Griffin, J.G. Liou and Sergio Speziale significantly improved this paper, and we gratefully acknowledge their comments.

Always consult and cite the final, published document. See http://www.minsocam.org or GeoscienceWorld

934
935

936 **Figure and Table Captions**
937

938 Figure 1. A. Geologic and tectonic domain map of Greenland showing the location of the
939 study region (white box) in West Greenland. B. The distribution of lithologic units,
940 structural features within the Nagssugtoqidian orogeny (NO), and the Nordre Strømfjord
941 shear zone (NSSZ). C. Sample locations for samples treated in this report. Sample
942 492042E is indicated in B, as well as the location of the study area (white box) depicted
943 in C.

944

945 Figure 2. Field photos of outcrops for areas associated with samples 123220 (A.) and
946 540521b (C.). Thin sections of the respective samples studied in this report are shown in
947 B. and D. Also shown are the locations on the thin sections of other figures in this report.

948

949 Figure 3. Garnets and inclusions in samples 159966 and 540521b. A. Photomicrograph
950 (plane light, true color) of garnet in 159966. Note the clear core, inclusion-rich mantle
951 and clear rim. B. Photomicrograph (plane light, black and white processed 3-D image) of
952 the inclusion-rich region shown in A. Note the aligned crystallographic form of the
953 inclusions. C. Photomicrograph (plane light, true color) of garnet in 540521b. D.
954 Photomicrograph (plane light, true color) of boxed area in C. E. Back-scattered electron
955 (BSE) image of inclusions in D. White is Ilm, black is Qtz. All inclusions in the inclusion
956 trains seen in C. consist of the same mineralogy.

957

Figure 4. Compositional characteristics of garnet in sample 123220. A., B. Electron microprobe (EMP) point traverse for atomic proportion (based on 12 O) of Fe (A.; dots and solid line), Mg (A.; circles and dashed line), Mn (B.; dots and solid line) and Ca (B.; circles and dashed line). Clear core and rim regions are indicated. C. LA-ICPMS spot analyses for Cr and Ti (clear core zone is indicated). Error bars are 1 sigma for Ti, based on counting statistics. Error bars for Cr are smaller than the circles. The distance scale uses a different origin for reference than that used in A. and B. D. LA-ICPMS analysis of rare earth element (REE) distributions (normalized to chondrites; Sun and McDonough, 1989) for the core, mantle (range indicated by double arrow) and rim of garnet. For comparison, garnet REE distributions from the Western Gneiss Region of Norway (Konrad-Schmolke et al., 2008), Himalayan majorities (Scambelluri et al., 2008) and South African kimberlites (Lazarov et al., 2012) are also shown. The locations of the LA-ICP-MS analyses are indicted by the stars in A; the two stars linked by double arrows span the mantle compositions indicated in D.

Figure 5. EMP analyses for pyroxenes and inclusions in sample 159966. A. Variation diagrams for the atomic proportions of Mg vs Fe. B. Variation diagrams for the atomic proportions of Ca vs Si. Unaltered Opx are indicated by solid dots. Compositions of inclusions are shown by gray dots. Boxes indicate the three end members, based on clustered analyses. The star indicates the computed composition for Opx exsolved from Grt, based on re-mixing of the inclusions in proportions inferred from observed relative abundances of each end member.

This is a preprint, the final version is subject to change, of the American Mineralogist (MSA)
Cite as Authors (Year) Title. American Mineralogist, in press.
(DOI will not work until issue is live.) DOI: http://dx.doi.org/10.2138/am.2014.4726

Figure 6. Atomic proportion of Al vs Si in Grt (on the basis of 12 O) from the indicated sources. The orange crosses are sample averages for all garnet analyses obtained from samples within the NSSZ since 1980. The red, green and black dots are the spot analyses for samples 123220, 540521b and 159966, respectively. The gray boxes indicate the garnet composition resulting from re-mixing of the indicated proportions of garnet and exsolved orthpyroxene for 159966. The dashed line indicates the Haggerty and Sautter (1991) trend for majorities, as a function of pressure (labeled tick marks).

Figure 7. Carbon (C) inclusions in garnet in 123220. The upper figure is a BSE image of the garnet with the C inclusions indicated by the boxes. Note that they only occur throughout the mantle region of the garnet. Lower right image is a reflected light photomicrograph of the large (right) and small (left) grains identified in Figure 8 as Grain 5 large and Grain 5 small, respectively. The middle lower figure is a photomicrograph of the same grains in plane polarized transmitted light, natural color. Note the well-defined faceted forms, particularly for the smaller inclusion. Lower left image is a photomicrograph (3-D, transmitted plane light, processed black and white) of the same inclusions as in the lower right image. The symmetry is cubic, with a well-developed hexagonal cross section in the small grain resulting from the thin section surface cutting the grain close to the (1.5 1.5 1.5) plane. Note also the decompression cracks radiating from the basal portion of the larger grain.

Figure 8. Raman spectra of C grains 1 (5pt8), 5 small (5pt3) and 5 large (5pt4-2 and 5pt7) indicated in the garnet shown in Figure 7. Reference spectral lines for diamond (blue

Always consult and cite the final, published document. See http://www.minsocam.org or GeoscienceWorld

This is a preprint, the final version is subject to change, of the American Mineralogist (MSA)
Cite as Authors (Year) Title. American Mineralogist, in press.
(DOI will not work until issue is live.) DOI: http://dx.doi.org/10.2138/am.2014.4726

line) and graphite (green lines) are also shown. The red line and shaded region are background garnet lines. The Raman spot spectrum for Grain 5 large (5pt4-2) was taken adjacent to the spot 5pt7, which was also in Grain 5 large.

Figure 9. Photomicrographs of rutile exsolution in garnet 540599. Upper image is crossed nichols, lower image is 3-D, transmitted plane light, processed black and white image from a region near that of the upper image. The angular relationships between the three orientations of needles is shown in the upper left box of the lower image. If the section were oriented such that the symmetry axis were exactly vertical (instead of slightly inclined), the angular relationship would be 120^{o}.

Figure 10. Pyroxene ternary diagram for samples 123220, 159966 and 540521b. See text for explanation. For 123220 and 159966 Cpx are indicated by squares and Opx by circles. All pyroxene analyses from sample 540521b are shown by circles, except for the labeled stars, which are discussed in the text.

Figure 11. BSE images of pyroxene textures in 159966. A. Cpx and Opx host grains detailed in B, C and D. Also shown are the linear contacts between crystals that parallel (100) and (001). B. Pyroxene lamellae OpxL1 and OpxL2 (light gray) in host Cpx (dark gray). C. Detail of pyroxene lamellae OpxL1 and OpxL3 (light gray) in host Cpx (dark gray). Also shown, for reference, are the orientations of (100) and (001). D. Detail of oxide and CpxL1 lamellae in host Opx.

Always consult and cite the final, published document. See http://www.minsocam.org or GeoscienceWorld

This is a preprint, the final version is subject to change, of the American Mineralogist (MSA)
Cite as Authors (Year) Title. American Mineralogist, in press.
(DOI will not work until issue is live.) DOI: http://dx.doi.org/10.2138/am.2014.4726

Figure 12. Images of pyroxene textures in 123220. A. Large Pgt grain with Rt lamellae and Fa-Qtz-(Fe-)Hd inclusions. Also shown are matrix Fa, Cpx and Qtz (plain light). B. Detail of Rt lamellae in Pgt (plain light). C. BSE detailed image of idiomorphic Fa-Qtz-(Fe-)Hd inclusion in A. Note the OpxL1 lamellae in the Fe-Hd. D. BSE detailed image of interface region between Fa and Fe-Hd with OpxL1 lamellae. Black arrow points to cuspate grain boundary discussed in text.

Figure 13. Pyroxene textures in 540521b. A. Photomicrograph (crossed nicols) of coarse Cpx lamellae (ferrosalites; CpxL-1) crosscutting Opx hosts and later generation Cpx lamellae. B. BSE detail of the finer Cpx lamellae, including the Omp + Cc lamellae. C. BSE image of details of pyroxene textures in A. Note the undulose, irregular grain margins of the CpxL-1 generation of lamellae and the sharp, linear grain margins of the later Cpx lamellae.

Figure 14. Reconstructed grain boundaries (upper figure) in the area depicted in Figure 13A (lower image). Red lines indicate the length, location and orientation of the CpxL-1 lamellae. The heavy black lines outline the original grain boundaries for the earliest homogeneous pyroxene phase required by the orientations and extent of the CpxL-1 lamellae. The dashed lines are the current Opx grain boundaries.

Figure 15. Olivine compositions for 123220 and 159966, in terms of Fe vs Mg (atoms per formula unit on the basis of 4 O). Ol-1 indicates the analyses for the olivines enclosed in the host garnet shown in Figure 7. Ol-2 indicates the field that encloses olivine analyses

Always consult and cite the final, published document. See http://www.minsocam.org or GeoscienceWorld

This is a preprint, the final version is subject to change, of the American Mineralogist (MSA)
Cite as Authors (Year) Title. American Mineralogist, in press.
(DOI will not work until issue is live.) DOI: http://dx.doi.org/10.2138/am.2014.4726

obtained for the Fa in the inclusion shown in Figure 12C. Ol-3 are analyses from olivines in the 123220 bulk rock.

Figure 16. Qtz needles in Fa, 123220. A. Transmitted light, crossed nicols of Fa crystal with areas with quartz fibers (indicated). Boxed region shows area depicted in B. Also shown are coexisting matrix Cpx and Qtz. B. Reflected light image of boxed area in A. Dark rods are Qtz fibers.

Figure 17. Pressure – temperature constraints for samples 123220, 159966 and 540521b. Orange and green circles are computed intersections for remixed mineral compositions using Brey and Köhler (1990) Cpx-Opx thermometry (computed as a function of pressure) and Opx-Grt barometry (computed as a function of temperature), for 123220 and 159966, respectively. The error bars bound the regions of intersections. The error bars for 540521b indicate the range of intersections for un-remixed compositions. The heavy red line is the Fs + Rt ⇔ Ilm + Qtz equilibrium, derived from Thermocalc (Holland and Powell, 2011). Also shown is the field, computed using Thermocalc, for the Fs ⇔ Fa + Qtz reaction, for the observed mineral compositions in sample 123220 (detailed in text). The field for the 3-phase pyroxene assemblage for 123220 is indicated by the pink field, based on Lindsley (1983). Dashed lines are the locus of pressure-dependent temperatures from Cpx-Opx thermometry on unmixed coexisting pyroxene lamellae for the indicated samples. The univariant equilibria for diamond ⇔ graphite is shown for reference. The fields for majorite (based on Sautter et al., 1991 and Ono, 1998) and ringwoodite + fayalite, as proxy for ahrensite + fayalite (Irifune and Ringwood,

Always consult and cite the final, published document. See http://www.minsocam.org or GeoscienceWorld

This is a preprint, the final version is subject to change, of the American Mineralogist (MSA)
Cite as Authors (Year) Title. American Mineralogist, in press.
(DOI will not work until issue is live.) DOI: http://dx.doi.org/10.2138/am.2014.4726

1987; Akaogi and Ito, 1989; Miyahara et al., 2008) are also shown. The green- and blue-boxed areas and the blue error bars are P-T constraints derived for garnet growth at the expense of amphibole and clinopyroxene (see text discussion for details). Orange, blue and green heavy lines indicate the simplest trajectories for the samples that also correspond to phase equilibria constraints. The P-T trajectories for other regional samples (468340, 492042E, 492045 and Marranguit) are shown for comparison.

Figure 18. P-T conditions for reported UHP terrains and the P-T loop for our UHP samples (red loop). The UHP trajectory for the samples described in this report are lumped together into a single trajectory (red loop), based on the assumption they experienced the same history. Gray ovals indicate discrete P-T constraints for the prograde and retrograde path, as discussed in the text. The yellow loop is the P-T trajectory for cold UHP metamorphism from Gilotti (2013). The other reported UHP terrains are: 1. Rhodope, Greece (Mposkos and Kostopoulos, 2001); 2. Saxonian Erzgebirge, Saidenbach reservoir (Massonne 2003; Hwang et al. 2007); 3. Garnet peridotite, North Qaidam, Tibetan Plateau (Song et al. 2004); 4. Garnet peridotite, Otrøy, Western Gneiss Region, Norway (Van Roermund et al. 2000); 5. Yangkou mafic-ultramafic complex, Sulu terrain, China (Zhang et al., et al. 2003); 6. Garnet peridotites, Czech Republic (Vrána, 2008); 7. Eclogite xenoliths, Premier Kimberlite (Dludla et al. 2006); 8. Felsic granulites, Bohemian Massif (Kröner et al., 2000; O'Brien and Rötzler, 2003; Hwang et al., 2007; Kotkavá et al. 2011); 9. Felsic granulite, Western Gneiss Region, Norway (Larsen et al., 1998); 10. Eclogite, Junan, Sulu Terrain (Zhang et al.,

Always consult and cite the final, published document. See http://www.minsocam.org or GeoscienceWorld

2003); 11. Kokchetav Massif (Hermann et al., 2001; Korsakov and Hermann, 2006); 12. Garnet xenocrysts, Garnet Ridge, Arizona (Wang et al. 1999).

Table 1. Mineral and rock compositions for samples 123220, 159966 and 540521b. The standard deviation (S.D.) shown for the LA-ICPMS analyses is the approximate average for all points analyzed.

1106
1107

1108 **REFERENCES**

1109

1110 Ague, J.J., and Eckert Jr., J.O. (2012) Precipitation of rutile and ilmenite needles in
1111 garnet: Implications for extreme metamorphic conditions in the Acadian Orogen, U.S.A.,
1112 American Mineralogist, 97, 840-855.

1113

1114 Akaogi, M., and Ito, E. (1989) Olivine-modified spinel-spinel transitions in the system
1115 Mg2SiO4-Fe2SiO4; Calorimetric measurements, thermochemical calculations and
1116 geophysical application. Journal of Geophysical Research, 94, 15,671-15,685.

1117

1118 Bak, J., Korstgård, J.A., Sørensen, K., 1975a. A major shear zone within the
1119 Nagssugtoqidian of West Greenland. Tectonophysics, 27, 191–209.

1120

1121 Bak, J., Sørensen, K., Grocott, J., Korstgård, J.A., Nash, D., Watterson, J., 1975b.
1122 Tectonic implications of Precambrian shear belts in western Greenland. Nature, 254,
1123 566–569.

1124

1125 Barron, B.J., Barron, L.M., and Duncan, G. (2005) Eclogitic and ultrahigh-pressure
1126 crustal garnets and their relationship to Phanerozoic subduction diamonds, Bingara area,
1127 New England Fold Belt, eastern Australia. Economic Geology, 100, 1565-1582.

1128

1129 Bozhilov, K.N., Green, H.W., and Dobrzhinetskaya, L.F. (2003) Quantitative 3D
1130 measurement of ilmenite abundance in Alpe Arami olivine: confirmation of high-pressure
1131 origin. American Mineralogist 88, 596–603.
1132
1133 Brey, G.P., and Köhler, T. (1990) Geothermobarometry in Four-Phase LherzolitesII. New
1134 thermobarometers and practical assessment of existing thermobarometers. Journal of
1135 Petrology, 31, 1353-1378.
1136
1137 Chopin, C., 1984. Coesite and pure pyrope in high-grade blueschists of the western Alps:
1138 a first record and some consequences. Contributions to Mineralogy and Petrology, 86,
1139 107-118.
1140
1141 Chopin, C. (2003) Ultrahigh-pressure metamorphism: tracing continental crust into the
1142 mantle. Earth and Planetary Science Letters, 212, 1-14.
1143
1144 Coats, J.S., Shaw, M.H., Smith, R.T., Rollin, K.E., Smith, C.G., and Fortey, N.J. (1996)
1145 Mineral exploration for gold and base metals in the Lewisian and associated rocks of the
1146 Glenelg area, north-west Scotland. Mineral Reconnaissance Programme Report, British
1147 Geological Survey, No. 140, 75 pp.
1148
1149 Coleman, R.G., Lee, D.E., Beatty, L.B., and Brannock, W.W. (1965) Eclogites and
1150 eclogites: their differences and similarities. Geological Society of America Bulletin, 76,
1151 483-508.

This is a preprint, the final version is subject to change, of the American Mineralogist (MSA)
Cite as Authors (Year) Title. American Mineralogist, in press.
(DOI will not work until issue is live.) DOI: http://dx.doi.org/10.2138/am.2014.4726

Connelly, J.N., and Mengel, F.C. (2000) Evolution of Archean components of the Nagssugtoqidian orogen, West Greenland. Geological Society of America Bulletin, 112, 747-763.

Connelly, J.N., van Gool, J.A.M., and Mengel, F.C. (2000) Temporal evolution of a deeply eroded orogen: the Nagssugtoqidian Orogen, West Greenland. Canadian Journal of Earth Sciences, 37, 1121-1142.

Davidson, L.M. (1979) Nagssugtoqidian granulite facies metamorphism in the Holsteinsborg region, West Greenland. Grønlands Geologiske Undersøgelse Rapport 89, 97-108.

Davies, G.R, Nixon, P.H., Pearson, D.G., and Obata, M. (1993) Tectonic implications of graphitized diamonds from the Ronda peridotite massif, southern Spain. Geology, 21, 471-474.

Day, H., and Mulcahy, S. R. (2007). Excess silica in omphacite and the formation of free silica in eclogite. Journal of Metamorphic Geology, 25, 37-50.

Always consult and cite the final, published document. See http://www.minsocam.org or GeoscienceWorld

1173 Dludla, S., le Roex, A.P., and Gurney, J.J. (2006) Eclogite xenoliths from the Premier
1174 kimberlite, South Africa: geochemical evidence for a subduction origin. South African
1175 Journal of Geology, 109, 353–368.
1176
1177 Dobrzhinetskaya, L.F., Green, H.W., and Wang, S. (1996) Alpe Arami: A peridotite
1178 massif from depths of more than 300 km. Science, 271, 1841–1846.
1179
1180 Dobrzhinetskaya, L.F., Bozhilov, K.N., and Green, H.W. (2000) The solubility of TiO_2 in
1181 olivine: Implication to the mantle wedge environment. Chemical Geology, 163, 325–338.
1182
1183 Ernst, W.G., and Liou, J.G. (2008) High- and ultrahigh-pressure metamorphism: Past
1184 results and future prospects. American Mineralogist, 93, 1771-1786.
1185
1186 Escher, A. (1970) The general structural pattern of the Nagssugtoqidian orogenic
1187 complex between Søndre Strømfjord and Jakobshavn, West Greenland. In: Colloquim
1188 on Nagssugtoqidian Geology. Geological Institute, Aarhus University, pp. 4–8.
1189
1190 Essene, E.J., and Fyfe, W.S. (1967) Omphacite in California metamorphic rocks.
1191 Contributions to Mineralogy and Petrology, 15, 1-23.
1192
1193 Garde, A.A., and Kalsbeek, F. (2006) Precambrian crustal evolution and Cretaceous-
1194 Paleogene faulting in West Greenland. Geological Survey of Denmark and Greenland
1195 Bulletin 11, 204 p.

Geiger, C.A., and Feenstra, A. (1997) Molar volumes of mixing of almandine-pyrope and almandine-spessartine garnets and the crystal chemistry and thermodynamic-mixing properties of the aluminosilicate garnets. American Mineralogist, 82, 571-581.

Gilotti, J.A. (2013) The realm of ultra-high pressure metamorphism. Elements 9, 255-260.

Glassley, W.E. (1983) Deep crustal carbonates as CO2 fluid sources: evidence from metasomatic reaction zones. Contributions to Mineralogy and Petrology, 84, 15–24.

Glassley, W.E. & Sørensen, K. (1980) Constant Ps-T amphibolite to granulite facies transition in Agto (West Greenland) metadolerites: implications and applications. Journal of Petrology, 21, 69–105.

Glassley, W.E., Korstgård, J.A., and Sørensen, K. (2007) Two tectonically significant enclaves in the Nordre Strømfjord shear zone at Ataneq, central West Greenland. Geological Survey of Denmark and Greenland Bulletin, 13, 49-52.

Glassley, W.E., Korstgård, J.A., and Sørensen, K. (2010) K-rich brine and chemical modification of the crust during continent–continent collision, Nagssugtoqidian Orogen, West Greenland. Precambrian Research, 180, 47-62.

1219 Griffin, W.L. (2008) Major transformations reveal Earth's deep secrets. Geology, 36, 95-
1220 96.
1221
1222 Griffin, W.L., Jensen, B.B. and Misra, S.N. (1971) Anomalously elongated rutile
1223 in eclogite-facies pyroxene and garnet. Norsk Geologisk Tidsskrift, 51, 177–185.
1224
1225 Haggerty, S.E., and Sautter, V. (1990) Ultradeep (greater than 300 kilometers) ultramafic
1226 upper mantle xenoliths. Science, 248, 993-996.
1227
1228 Hansen, B.F. (1979) Some charnockitic rocks in the Nagssugtoqidian of West Greenland.
1229 Rapport Grønlands Geologiske Undersøgelse, 89, 85–96.
1230
1231 Harley, S.L. (1987) A pyroxene-bearing meta-ironstone and other pyroxene-granulties
1232 from Tonagh Island, Enderby Land, Antarctica: further evidence for very high
1233 temperature (>980^{o}C) Archaean regional metamorphism in the Napier Complex. Journal
1234 of Metamorphic Geology, 5, 341-356.
1235
1236 Hazen, R.M., Downs, R.T., Finger, L.W., and Ko, J. (1993) Crystal chemistry of
1237 ferromagnesian silicate spinels: Evidence for Mg-Si disorder. American Mineralogist, 78,
1238 1320-1323.
1239
1240 Hermann, J., Rubatto, D., Korsakov, A., Shatsky, V.S. (2001) Multiple growth during

This is a preprint, the final version is subject to change, of the American Mineralogist (MSA)
Cite as Authors (Year) Title. American Mineralogist, in press.
(DOI will not work until issue is live.) DOI: http://dx.doi.org/10.2138/am.2014.4726

fast exhumation of diamondiferous deeply subducted continental crust (Kokchetav Massif, Kazakhstan). Contributions to Mineralogy and Petrology, 141, 66–82.

Hickman, M.H., and Glassley, W.E. (1984) The role of metamorphic fluid transport in the Rb-Sr isotopic resetting of shear zones: evidence from Nordre Strømfjord, West Greenland. Contributions to Mineralogy and Petrology, 87, 265-281.

Holland. T.J.B. and Powell, R. (1990) An enlarged and updated internally consistent thermodynamic dataset with uncertainties and correlations: the system K2O-Na2O-CaO-MgO-MnO-FeO-Fe2O3-Al2O3-TiO2-SiO2-C-H2-O2. Journal of Metamorphic Geology, 8, 89-124.

Holland, T., and Powell, R. (2011) An improved and extended internally consistent thermodynamic dataset for phases of petrological interest, involving a new equation of state for solids. Journal of Metamorphic Geology, 29, 333-383

Holness, M.B., Stripp, G., Humphreys, M.C.S., Veksler, I.V., Nielsen, T.F.D., and Tegner, C. (2011) Silicate liquid immiscibility within the crystal mush: Late-stage magmatic microstructures in the Skaergaard intrusion, East Greenland. Journal of Petrology, 52, 175-222.

Always consult and cite the final, published document. See http://www.minsocam.org or GeoscienceWorld

Hwang, S.L., Yui, T.F., Chu, H.T., Shen, P., Schertl, H.P., Zhang, R.Y., and Liou, J.G. (2007) On the origin of oriented rutile needles in garnet from UHP eclogites. Journal of Metamorphic Geology, 25, 349–362.

Hyslop, E.V. Valley, J.W., Johnson, C.M., and Beard, B.L. (2008) The effects of metamorphism on O and Fe isotope compositions in the Biwabik Iron Formation, northern Minnesota. Contributions to Mineralogy and Petrology, 155, 313-328.

Irifune, T., and Ringwood, A.E. (1987) Phase transformations in a harzburgite composition to 26 GPa: implications for dynamical behaviour of the subducting slab. Earth and Planetary Science Letters, 86, 365-376.

Kalsbeek, F., Pidgeon, R.T., and Taylor, P.N. (1987) Nagssugtoqidian mobile belt of West Greenland: a cryptic 1850 Ma suture between two Arcaean continents - chemical and isotopic evidence. Earth and Planetary Science Letters, 85, 365-385.

Kalsbeek, F., and Nutman, A.P. (1996) Anatomy of the Early Proterozoic Nagssugtoqidian orogen, West Greenland explored by reconnaissance SHRIMP U-Pb zircon dating. Geology, 24, 515-518.

Konrad-Schmolke, M., Zack, T., O'Brien, P.J., and Jacob, D.E. (2008) Combined thermodynamic and rare earth element modelling of garnet growth during subduction:

1284 Examples from ultrahigh-pressure eclogite of the Western Gneiss Region, Norway. Earth
1285 and Planetary Science Letters, 272, 488-498.
1286
1287 Korsakov, A.V., Hermann, J., 2006. Silicate and carbonate melt inclusions associated
1288 with diamonds in deeply subducted carbonate rocks. Earth and Planetary Science Letters,
1289 241, 104–118.
1290
1291 Korstgård, J.A. (1979) Nagssugtoqidian Geology. Grønlands Geologiske Undersøgelse
1292 Rapport 89, 146 p.
1293
1294 Kotkavá, J., O'Brien, P.J., and Ziemann, M.A. (2011) Diamond and coesite discovered in
1295 Saxony-type granulite: Solution to the Variscan garnet peridotite enigma. Geology, 39,
1296 667–670.
1297
1298 Kröner, A., O'Brien, P.J., Nemchin, A.A., and Pidgeon, R.T. (2000) Zircon ages for high
1299 pressure granulites from South Bohemia, Czech Republic, and their connection to
1300 Carboniferous high temperature processes. Contributions to Mineralogy and Petrology,
1301 138, 127–142.
1302
1303 Larsen, R.B., Eide, E.A., and Burke, E.A.J. (1998) Evolution of metamorphic volatiles
1304 during exhumation of microdiamond-bearing granulites in the Western Gneiss Region,
1305 Norway. Contributions to Mineralogy and Petrology, 133, 106-121.
1306

1307 Lazarov, M., Brey, G.P., and Weyer, S. (2012) Evolution of the South African mantle —
1308 A case study of garnet peridotites from the Finsch diamond mine (Kaapvaal craton); part
1309 1: Inter-mineral trace element and isotopic equilibrium. Lithos, 154, 193-209.
1310
1311 Lindsley, D.H. (1983) Pyroxene thermometry. American Mineralogist, 68, 477-493.
1312
1313 Massonne, H.J. (2003) A comparison of the evolution of diamondiferous quartz-rich
1314 rocks from the Saxonian Erzgebirge and the Kokchetav Massif: are so-called
1315 diamondiferous gneisses magmatic rocks? Earth and Planetary Science Letters, 216, 347–
1316 364.
1317 Mazur, S., Anczkiewicz, R., Szczepanski, J., van Gool, J.A.M., and Thirlwall, M. (2012)
1318 Paleoproterozoic metamorphism and cooling of the northern Nagssugtoqidian orogeny,
1319 West Greenland. Precambrian Research, 196-197, 171-192.
1320 Mazzucchelli M., Rivalenti G., Vannucci R., Bottazzi P., Ottolini L., Hofmann A.W.,
1321 Sinigoi S., Demarchi G. (1992) Trace element distribution between clinopyroxene and
1322 garnet in gabbroic rocks of the deep crust: An ion microprobe study. Geochimica et
1323 Cosmochimica Acta, 56, 2371-2385.
1324 Mengel, F.C. (1983) Chemistry of coexisting mafic minerals in granulite facies
1325 amphibolites from West Greenland: clues to conditions of metamorphism. Neues
1326 Jahrbuch für Mineralogie Abhandlungen 147, 315–340.
1327

Miyahara, M., El Gorsey, A., Ohtani, E., Nagase, T., Nishijima, M., Vashaei, Z., Ferroir, T., Gillet, P., Dubrovinsky, L., and Simionovici, A. (2008) Evidence for fractional crystallization of wadsleyite and ringwoodite from olivine melts in chondrules entrained in shock-melt veins. Proceedings of the National Academy of Sciences 105, 8542-8547.

Morimoto, N., Fabries, J., Ferguson, A.K., Ginzburg, I.V., Ross, M., Seifert, F.A., Zussman, J. Aoki, K., and Gottardi, G. (1988) Nomenclature of pyroxenes. American Mineralogist, 73, 1123-1133.

Mposkos, E.D., and Kostopoulos, D.K. (2001) Diamond, former coesite and supersilicic garnet in metasedimentary rocks from the Greek Rhodope: a new ultrahigh-pressure metamorphic province established. Earth and Planetary Science Letters, 192, 497-506.

Nutman, A.P., Kalsbeek, F., Marker, M., van Gool, J.A.M. & Bridgwater, D. (1999) U-Pb zircon ages of Kangâmiut dykes and detrital zircons in metasediments in the Palaeoproterozoic Nagssugtoqidian Orogen (West Greenland). Clues to the pre-collisional history of the orogen. Precambrian Research, 93, 87–104.

O'Brien, P.J., and Rötzler, J. (2003) High-pressure granulites: formation, recovery of peak conditions and implications for tectonics. Journal of Metamorphic Geology, 21, 3–20.

Ollila, P.W., Jaffe, H.W., and Jaffe, E.B. (1988) Pyroxene exsolution: An indicator of

high-pressure igneous crystallization of pyroxene-bearing quartz syenite gneiss from the High Peaks region of the Adirondack Mountains. American Mineralogist, 73, 261-273.

Ono, S., (1998) Stability limits of hydrous minerals in sediment and mid-ocean ridge basalt compositions: Implications for water transportin subduction zones. Journal of Geophysical Research, 103, 18,253-18,267.

Paton, C., Hellstrom, J., Paul, B., Woodhead, J., and Hergt, J. (2011) Iolite: Freeware for the visualisation and processing of mass spectrometric data: Journal of Analytical Atomic Spectrometry, v. 26, no. 12, p. 2508.

Robinson, P., Jaffe, H.W., Ross, M., and Klein, C. Jr. (1971) Orientation of exsolution lamellae in clinopyroxene and clinoamphiboles: Consideration of optimal phase boundaries. American Mineralogist, 56, 909-939.

Sautter, V., Haggerty, S.E. and Field, S. (1991) Ultradeep (>300 Kilometers) ultramafic xenoliths: Pterological evidence from the transition zone. Science, 252, 827-830.

Scott, D., Marker, M., Gauthier, G., Stecher, O., Whitehouse, M., Bridgwater, D., van Gool, J. & Mengel, F.C. (1998) Age of deposition, provenance and tectonic setting of metasedimentary rocks in the Paleoproterozoic Nagssugtoqidian orogen, West Greenland. Lithoprobe Report 68, 148–149.

This is a preprint, the final version is subject to change, of the American Mineralogist (MSA)
Cite as Authors (Year) Title. American Mineralogist, in press.
(DOI will not work until issue is live.) DOI: http://dx.doi.org/10.2138/am.2014.4726

1374 Scambelluri, M., Pettke, T., and van Roermund, H.L.M. (2008) Majoritic garnets monitor
1375 deep subduction fluid flow and mantle dynamics: Geology, 36, p. 59–62.
1376
1377 Schmädicke, E., and Evans, B.W. (1997) Garnet-bearing ultramafic rocks from the
1378 Erzgebirge, and their relation to other settings in the Bohemian Massif. Contributions to
1379 Mineralogy and Petrology, 127, 57-74.
1380
1381 Smith, D. (1974) Pyroxene-Olivine-Quartz Assemblages in Rocks Associated with the
1382 Nain Anorthosite Massif, Labrador. Journal of Petrology, 15, 58-78.
1383
1384 Smith, D.C., and Godard, G. (2013) A Raman spectroscopic study of diamond and
1385 disordered sp3-carbon in the coesite-bearing Straumen eclogite pod, Norway. Journal of
1386 Metamorphic Geology, 31, 19-33.
1387
1388 Song, S., Zhang, L., and Niu, Y. (2004) Ultra-deep origin of garnet peridotite from the
1389 North Qaidam ultrahigh-pressure belt, northern Tibetan Plateau, NW China. American
1390 Mineralogist, 89, 1330–1336.
1391
1392 Sun S.-S., and McDonough W. F. (1989) Chemical and isotopic systematics of oceanic
1393 basalts: implications for mantle compositions and processes. In Geol. Soc. Spec. Pub.
1394 (eds. N. M. Saunders and A. D. Norris), pp. 313–345.
1395
1396 Sørensen, K. (1983) Growth and dynamics of the Nordre Strømfjord shear zone. Journal
1397 of Geophysical Research, 88, 3419–3437.

Always consult and cite the final, published document. See http://www.minsocam.org or GeoscienceWorld

Taylor, P.N., and Kalsbeek, F. (1990) Dating the metamorphism of Precambrian marbles: Examples from Proterozoic mobile belts in Greenland. Chemical Geology, 86, 21-28.

Tilley, C.E., 1936. Eulysites and related rock types from Loch Duich, Ross-shire. Mineralogical Magazine, 24, 331-342.

Tiwari, R.N., Ishihara, M., Tiwari, J.N. and Yoshimura, M. (2012) Synthesis of grapheme film from fullerene rods. Chemical Communications, 48, 3003-3005.

van Gool, J.A.M., Connelly, J.N., Marker, M., and Mengel, F.C. (2002) The Nagssugtoqidian Orogen of West Greenland: tectonic evolution and regional correlations from a West Greenland perspective. Canadian Journal of Earth Sciences, 39, 665-686

Vannucci R., Ottolini L., Bottazzi P., Downes H., Dupuy C. (1994) INAA, IDMS and SIMS comparative REE investigations of clinopyroxenes from mantle xenoliths with different textures. Chemical Geology, 118, 85-108.

Van Roermund, H.L.M., Drury, M.R., Barnhoorn, A., and de Ronde, A.A. (2000) Super-silicic garnet microstructures from an orogenic garnet peridotite, evidence for an ultra-deep (>6 GPa) origin. Journal of Metamorphic Geology, 18, 135-147.

Vrána, S. (2008) Mineral inclusions in pyrope from garnet peridotites, Kolin area, central Czech Republic. Journal of Geosciences 53, 17-30.

This is a preprint, the final version is subject to change, of the American Mineralogist (MSA)
Cite as Authors (Year) Title. American Mineralogist, in press.
(DOI will not work until issue is live.) DOI: http://dx.doi.org/10.2138/am.2014.4726

1420 Wang, L., Essene, E.J., and Zhang, Y. (1999) Mineral inclusions in pyrope crystals from
1421 Garnet Ridge, Arizona, USA: Implications for processes in the upper mantle.
1422 Contributions to Mineralogy and Petrology, 135, 164-178.
1423
1424 Whitehouse, M.J., Kalsbeek, F., and Nutman, A.P. (1998) Crustal growth and crustal
1425 recycling in the Nagssugtoqidian orogen of West Greenland: Constraints from radiogenic
1426 isotope systematics and U-Pb zircon geochronology. Precambrian Research 91, 365-381.
1427
1428 Whitney, D.L. and Evans, B.W. (2010) Abbreviations for names of rock-forming
1429 minerals. American Mineralogist, 95, 185-187.
1430
1431 Willigers, B.J.A., Krogstad, E.J., and Wijbrans, J.R. (2001) Comparison of
1432 thermochronometers in a slowly cooled granulite terrain: Nagssugtoqidian orogeny, West
1433 Greenland. Journal of Petrology, 42, 1729-1749.
1434
1435 Ye, K., Cong, B., and Ye, D. (2000) The possible subduction of continental material to
1436 depths greater than 200 km. Nature 407, 734-736.
1437
1438 Zhang, R.Y., and Liou, J.G. (1999) Exsolution lamellae in minerals from ultrahigh-
1439 pressure rocks. International Geology Review 41, 981-993.
1440

Always consult and cite the final, published document. See http://www.minsocam.org or GeoscienceWorld

This is a preprint, the final version is subject to change, of the American Mineralogist (MSA)
Cite as Authors (Year) Title. American Mineralogist, in press.
(DOI will not work until issue is live.) DOI: http://dx.doi.org/10.2138/am.2014.4726

1441 Zhang, R.Y., Zhai, S.M., Fei, Y.W., and Liou, J.G. (2003) Titanium solubility in
1442 coexisting garnet and clinopyroxene at very high pressure: the significance of exsolved
1443 rutile in garnet. Earth and Planetary Science Letters, 216, 591-601.
1444

Always consult and cite the final, published document. See http://www.minsocam.org or GeoscienceWorld

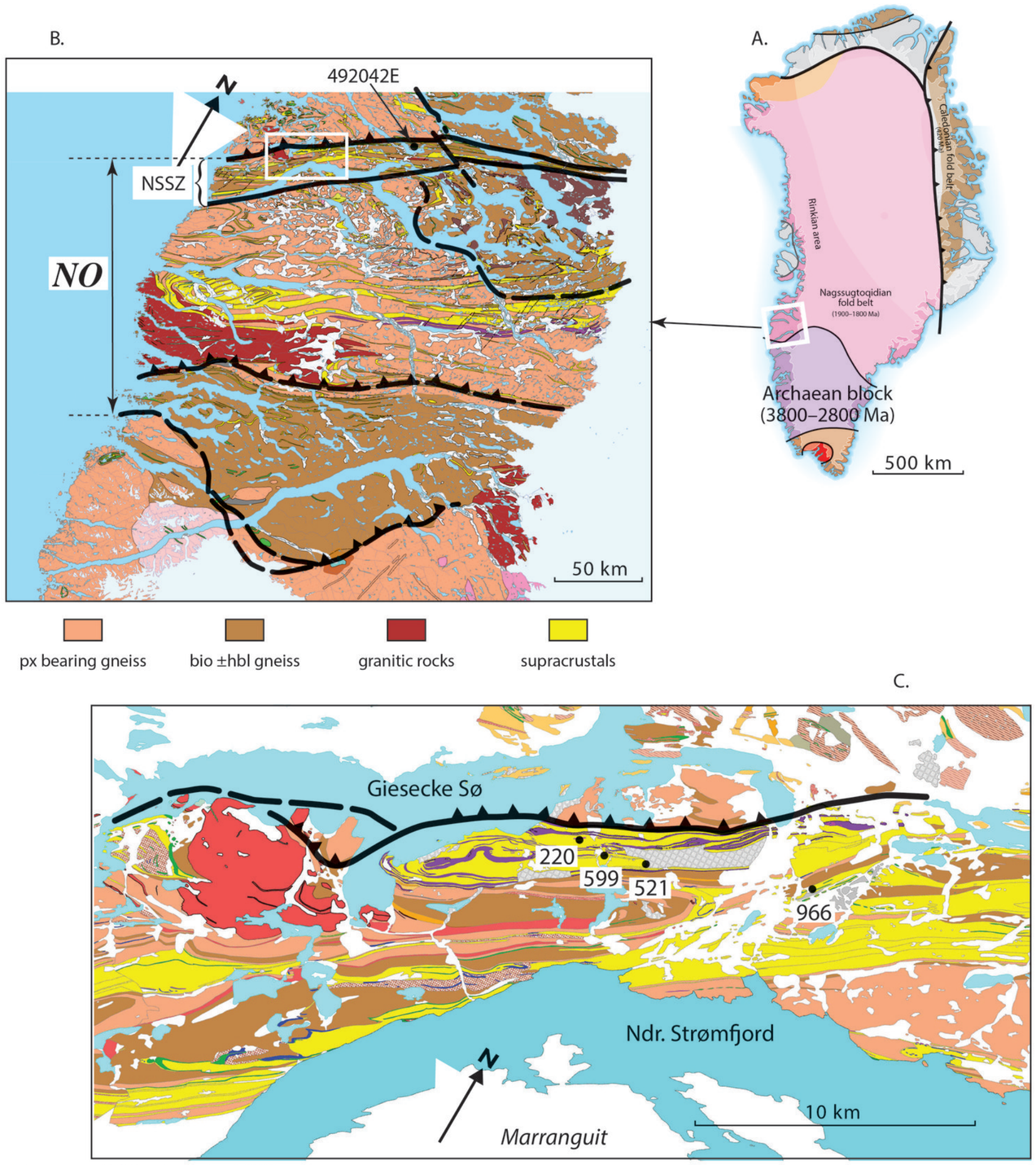

Glassley et al., West Greenland UHP *Figure 1*

A.

123220

B.

C.

540521b

D.

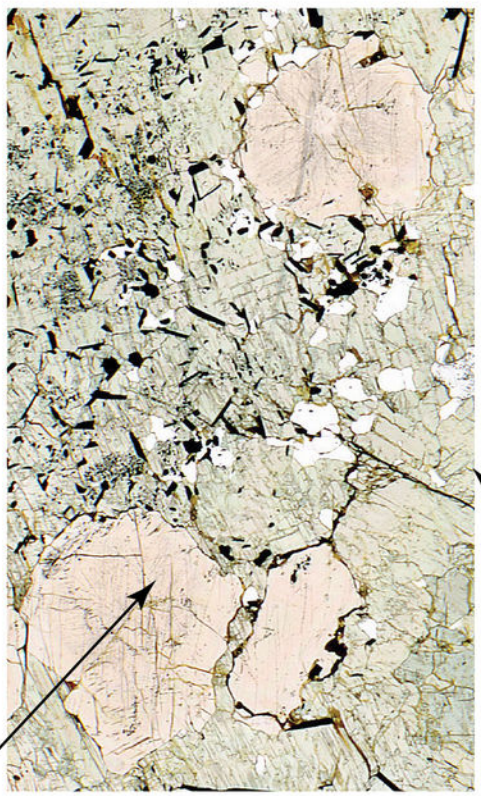

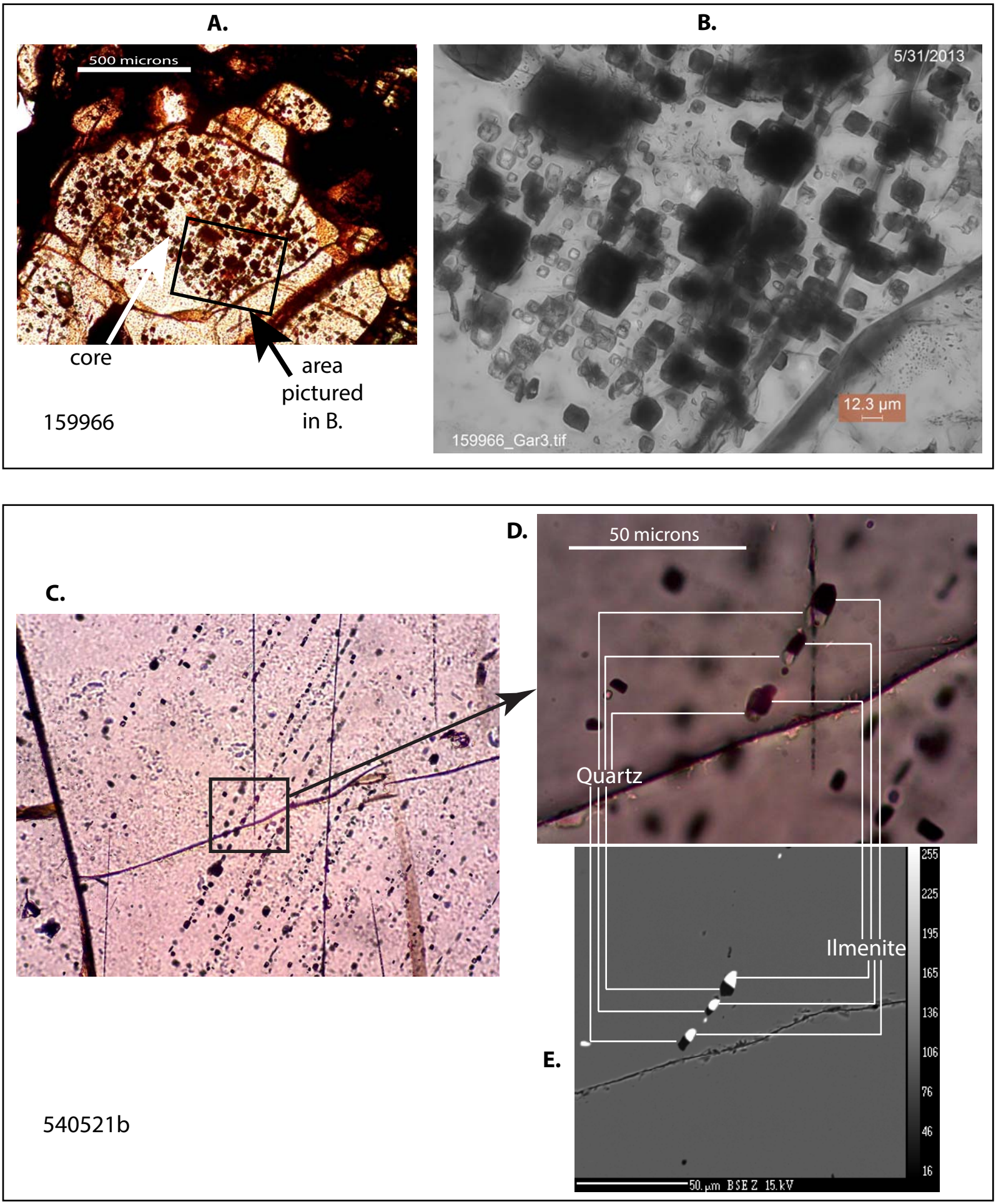

Glassley et al., West Greenland UHP *Figure 3*

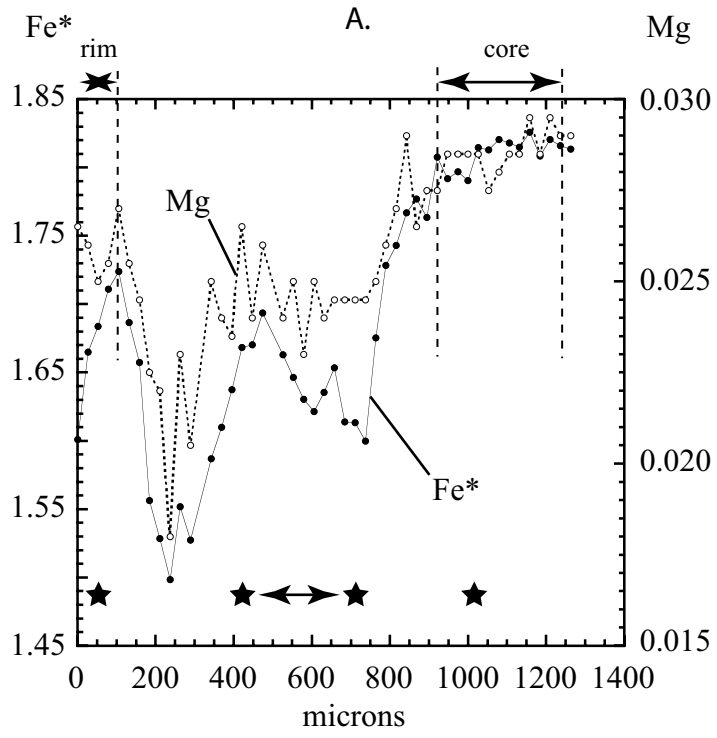
A.
Fe*
Mg
rim
core
Mg
Fe*
1.85
1.75
1.65
1.55
1.45
0.030
0.025
0.020
0.015
0
200
400
600
800
1000
1200
1400
microns

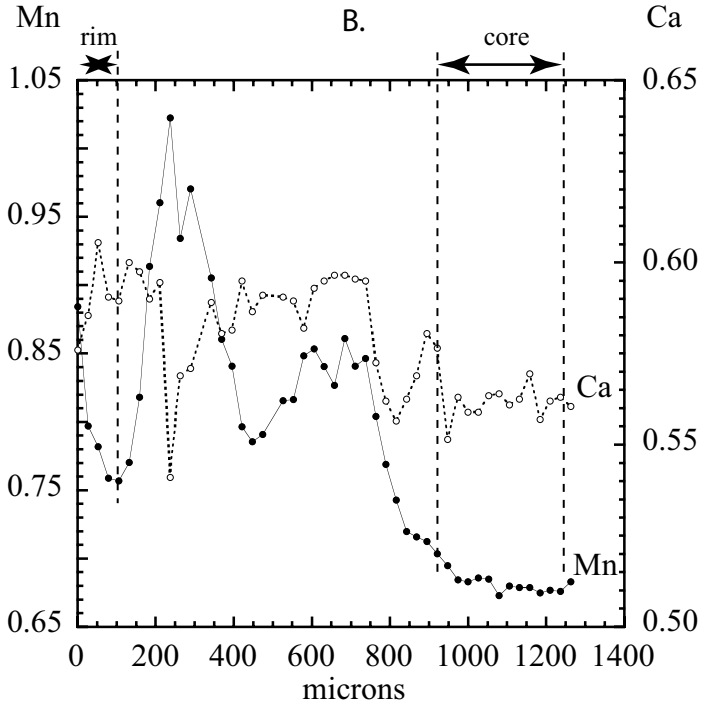
B.
Mn
Ca
rim
core
Ca
Mn
1.05
0.95
0.85
0.75
0.65
0.65
0.60
0.55
0.50
0
200
400
600
800
1000
1200
1400
microns

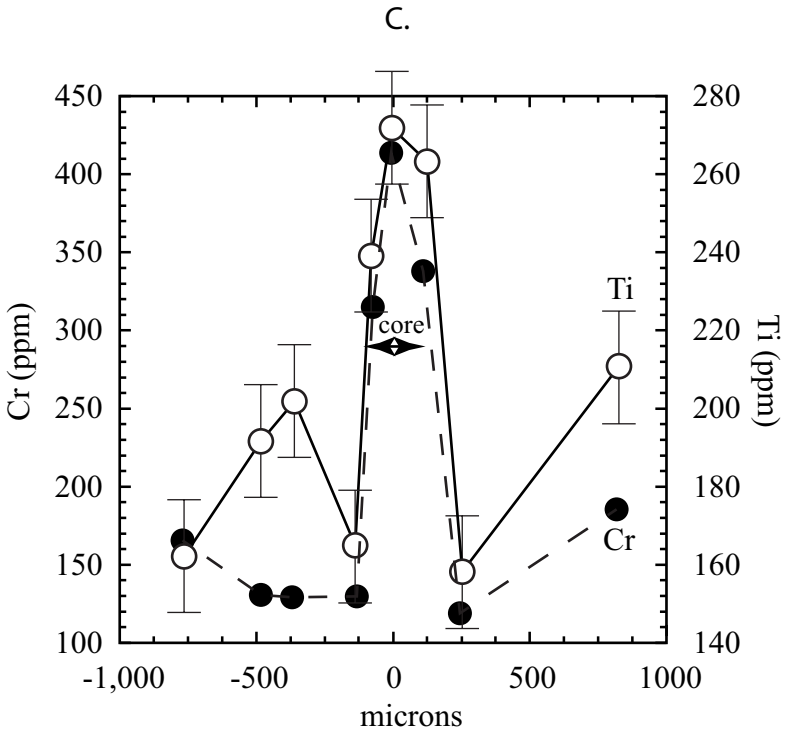
C.
Cr (ppm)
Ti (ppm)
core
Ti
Cr
450
400
350
300
250
200
150
100
280
260
240
220
200
180
160
140
-1,000
-500
0
500
1000
microns

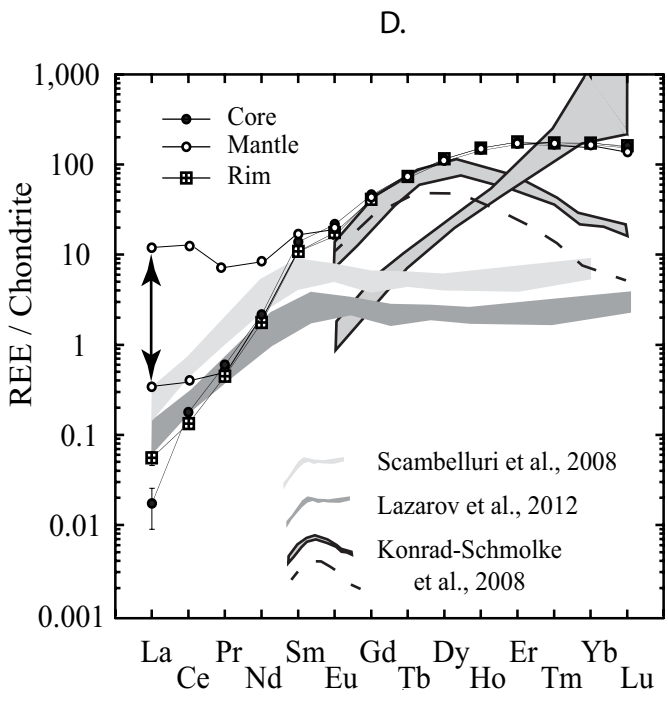
D.
REE / Chondrite
Core
Mantle
Rim
Scambelluri et al., 2008
Lazarov et al., 2012
Konrad-Schmolke
et al., 2008
1,000
100
10
1
0.1
0.01
0.001
La
Ce
Pr
Nd
Sm
Eu
Gd
Tb
Dy
Ho
Er
Tm
Yb
Lu

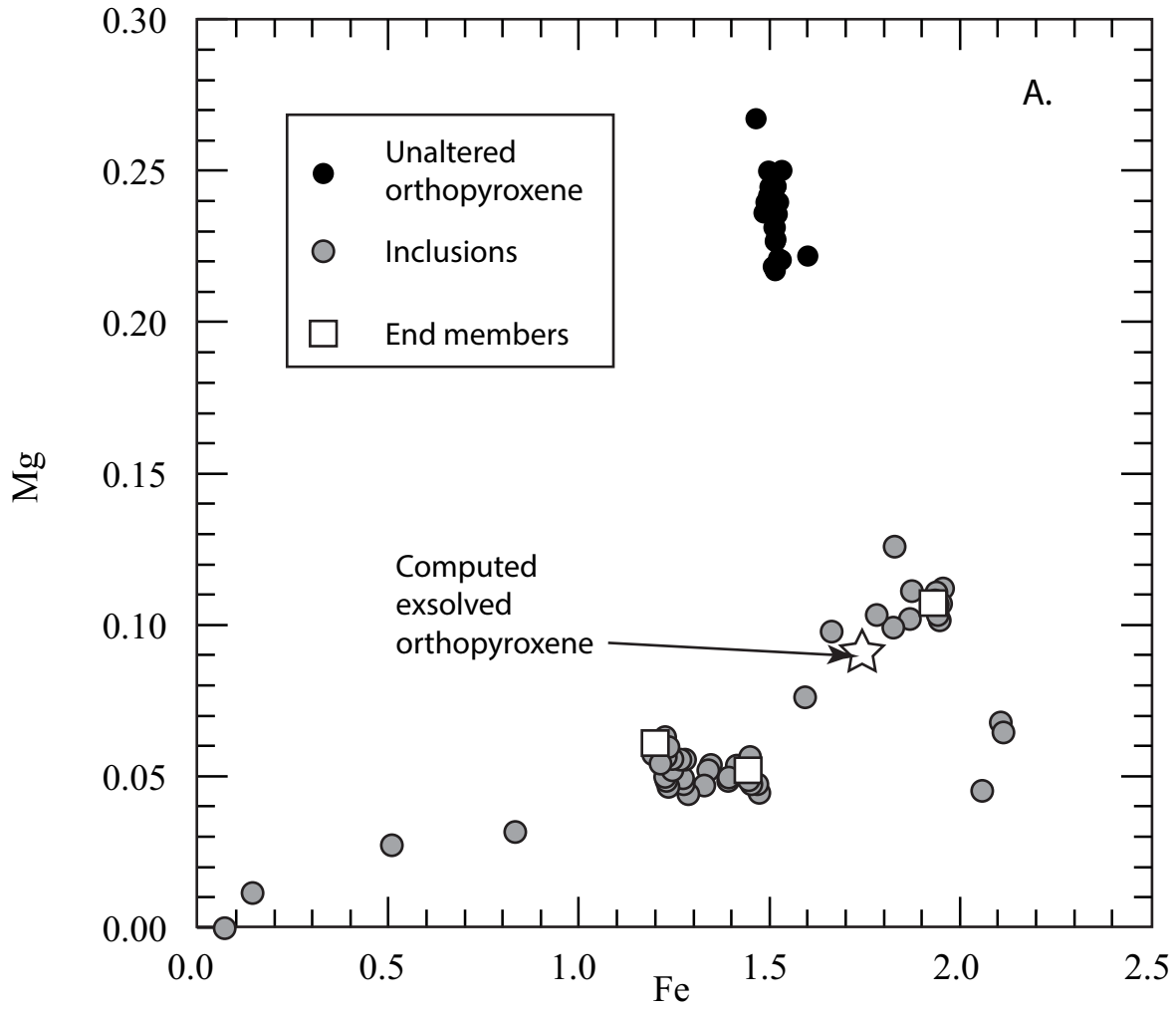
A.
Unaltered orthopyroxene
Inclusions
End members
Computed exsolved orthopyroxene
Mg
Fe
0.00
0.05
0.10
0.15
0.20
0.25
0.30
0.0
0.5
1.0
1.5
2.0
2.5

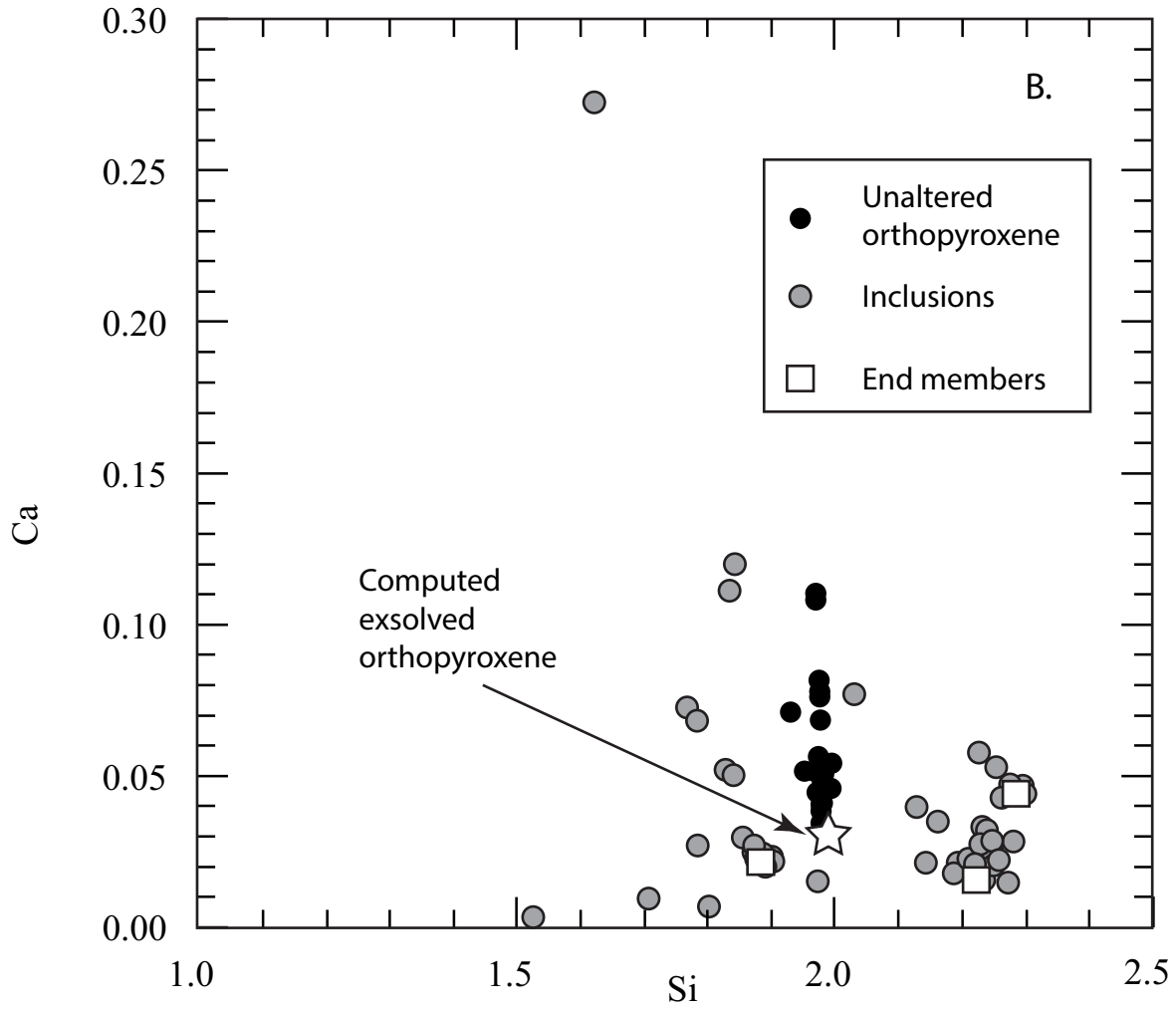
B.
Unaltered orthopyroxene
Inclusions
End members
Computed exsolved orthopyroxene
Ca
Si
0.00
0.05
0.10
0.15
0.20
0.25
0.30
1.0
1.5
2.0
2.5

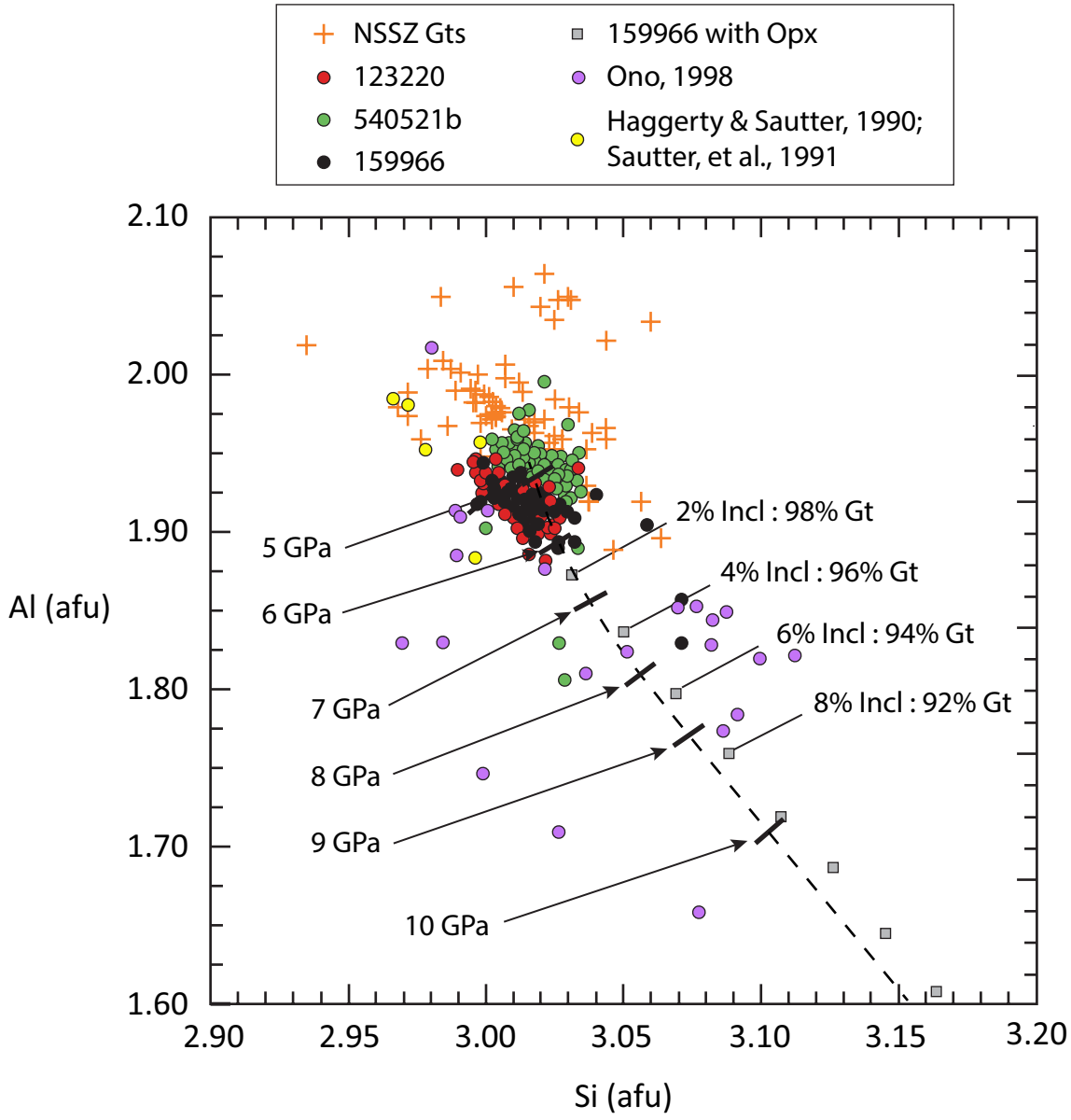
NSSZ Gts
123220
540521b
159966
159966 with Opx
Ono, 1998
Haggerty & Sautter, 1990; Sautter, et al., 1991
2.10
2.00
1.90
1.80
1.70
1.60
Al (afu)
2.90
2.95
3.00
3.05
3.10
3.15
3.20
Si (afu)
5 GPa
6 GPa
7 GPa
8 GPa
9 GPa
10 GPa
2% Incl : 98% Gt
4% Incl : 96% Gt
6% Incl : 94% Gt
8% Incl : 92% Gt

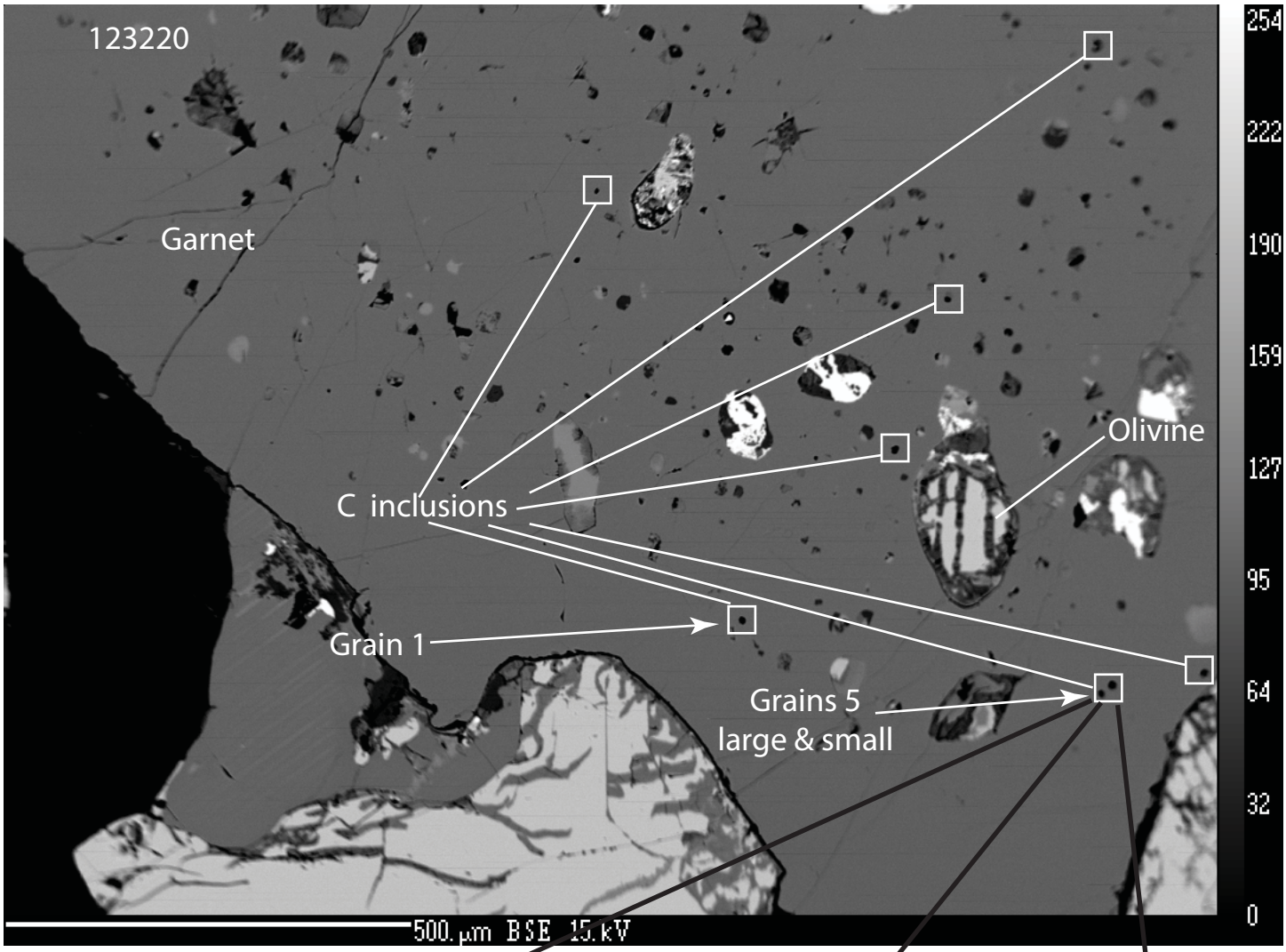

Transmitted light
stacked focus, B&W

Transmitted light
surface focus, true color

Reflected light
surface focus, true color

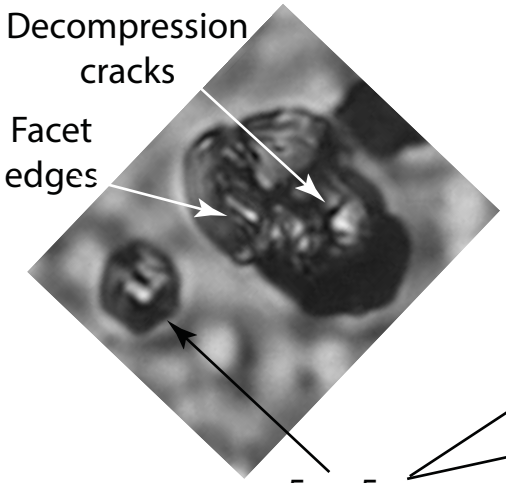

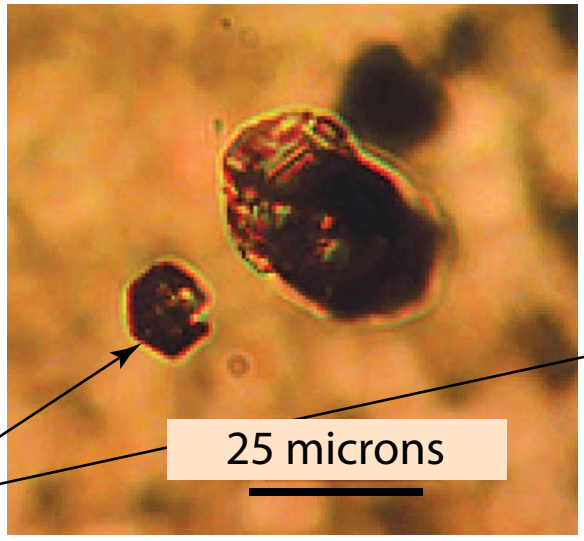

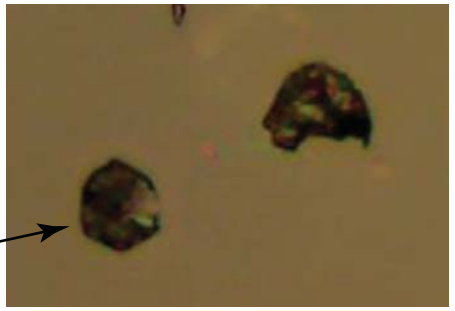

5µ x 5µ
faceted
cubic
form

Grains 5 large and small

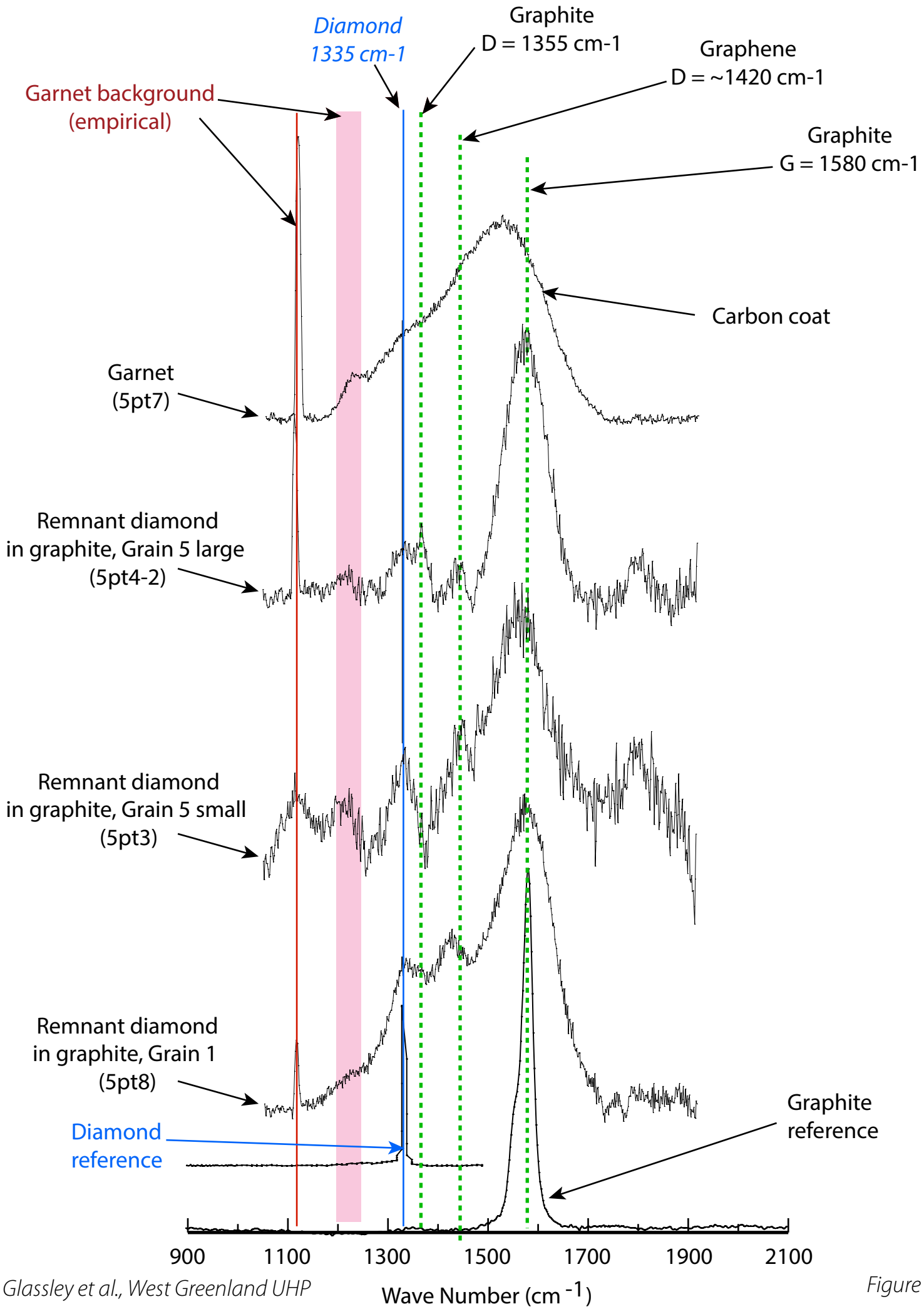
Diamond
1335 cm-1
Graphite
D = 1355 cm-1
Graphene
D = ~1420 cm-1
Garnet background
(empirical)
Graphite
G = 1580 cm-1
Carbon coat
Garnet
(5pt7)
Remnant diamond
in graphite, Grain 5 large
(5pt4-2)
Remnant diamond
in graphite, Grain 5 small
(5pt3)
Remnant diamond
in graphite, Grain 1
(5pt8)
Diamond
reference
Graphite
reference
900
1100
1300
1500
1700
1900
2100
Wave Number (cm -1)

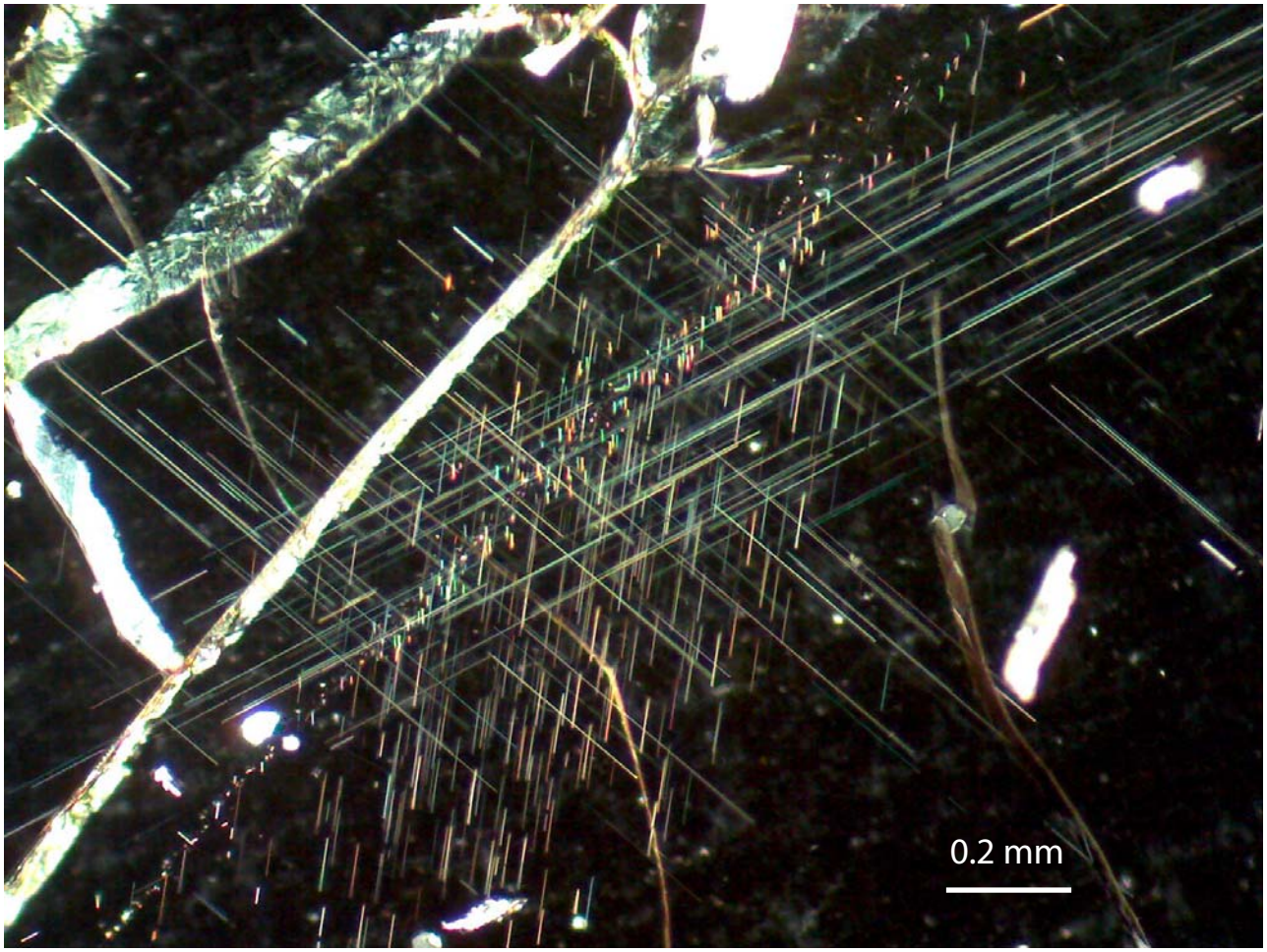
0.2 mm

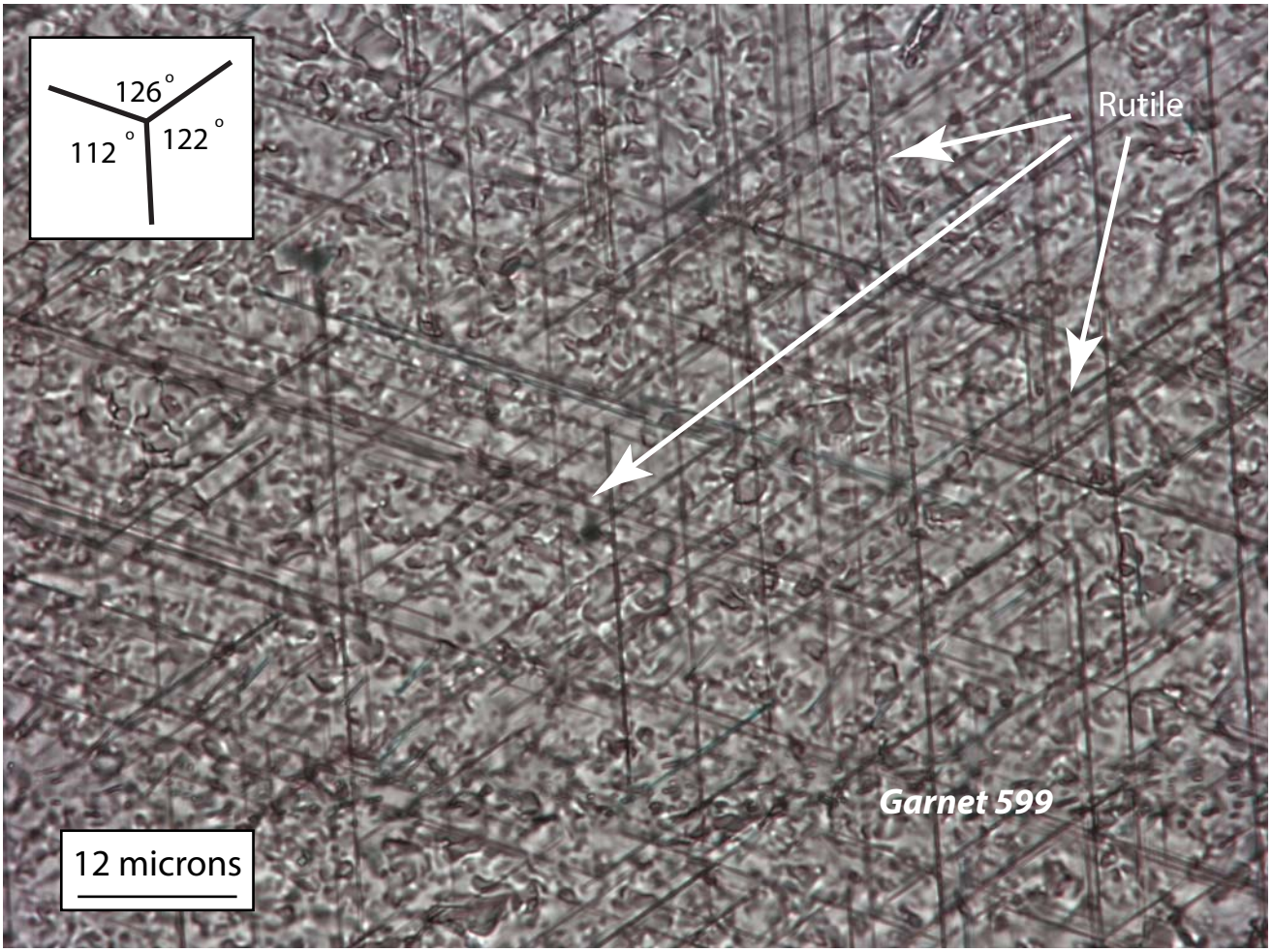
126°
112°
122°
Rutile
Garnet 599
12 microns

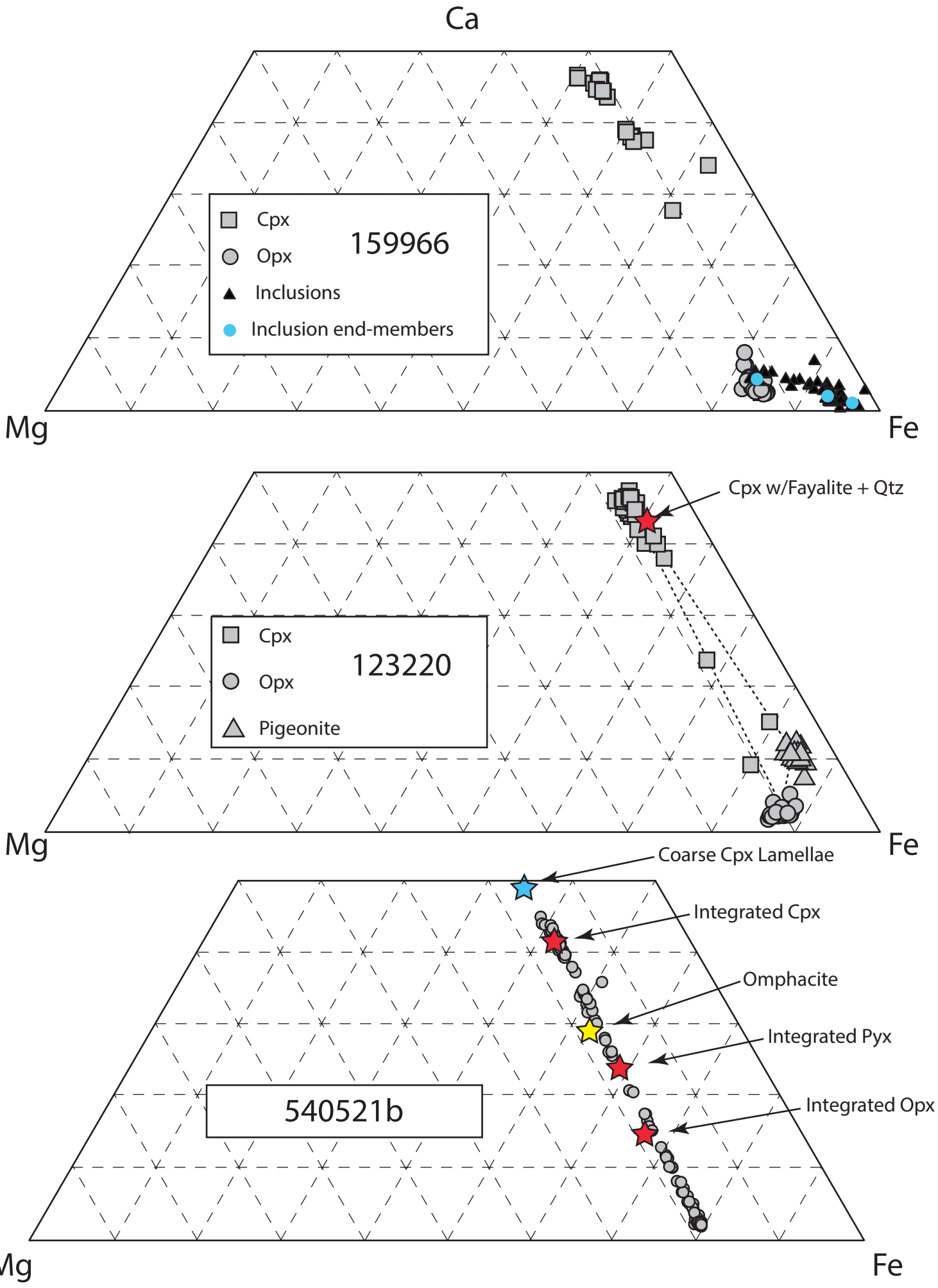

Glassley et al., West Greenland UHP

Figure 10

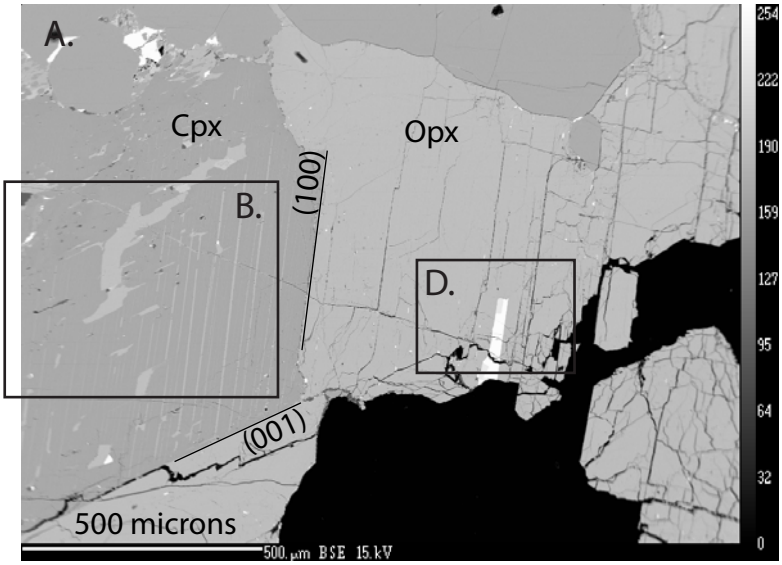

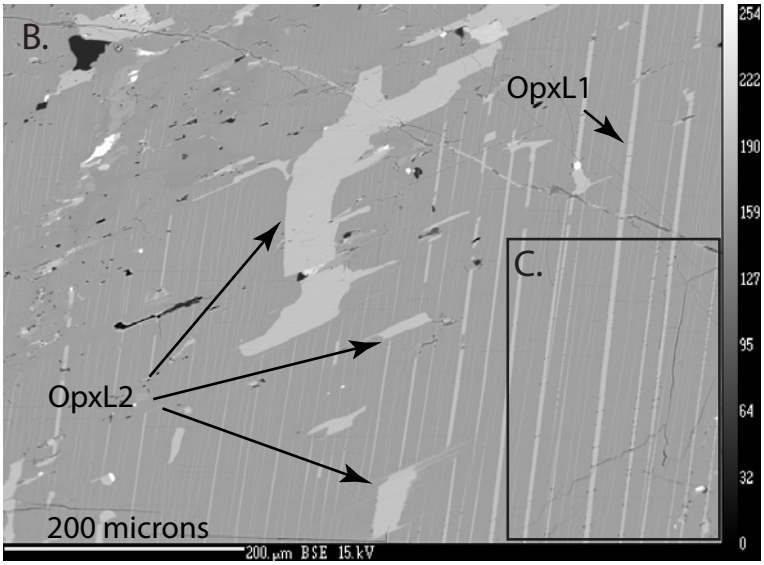

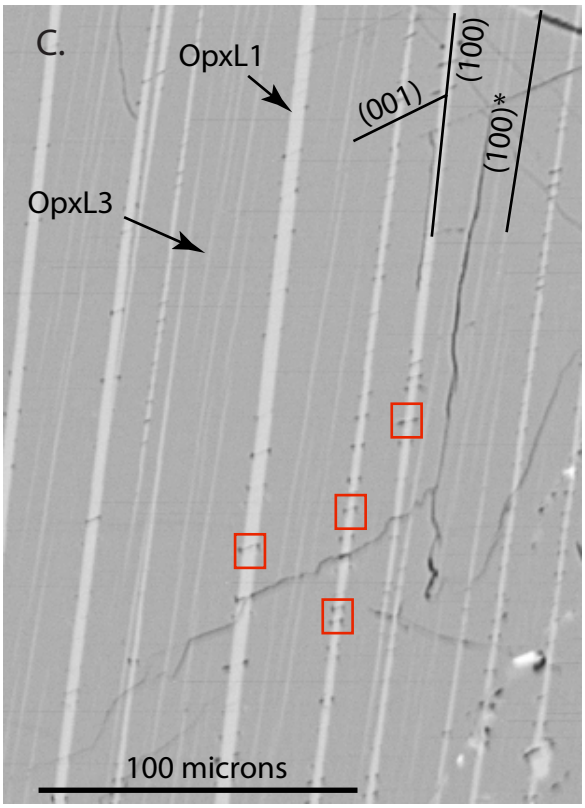

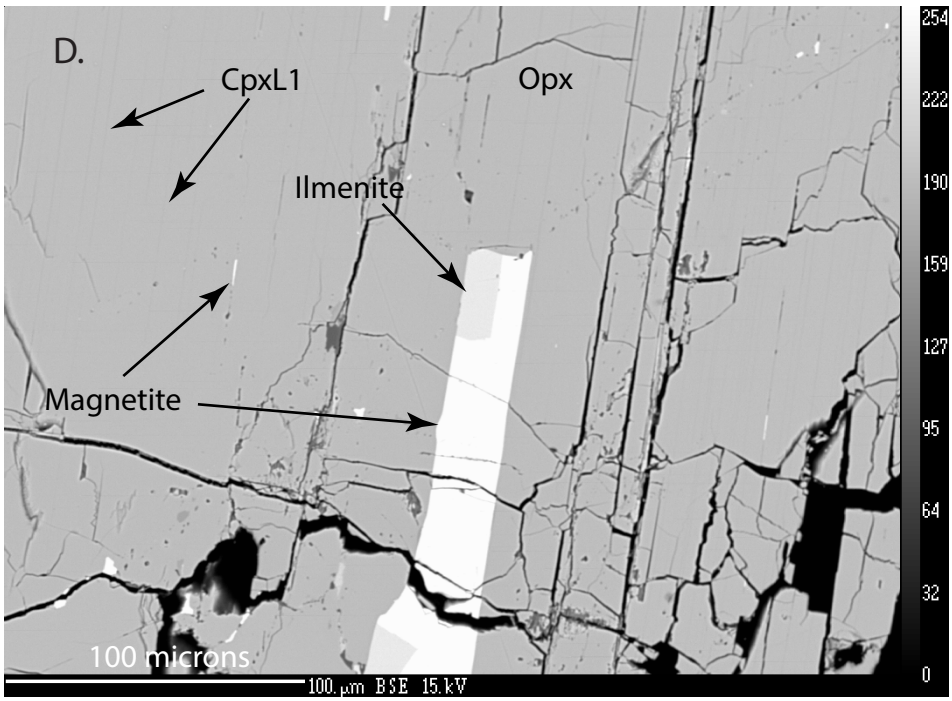

Glassley et al., West Greenland UHP *Figure 11*

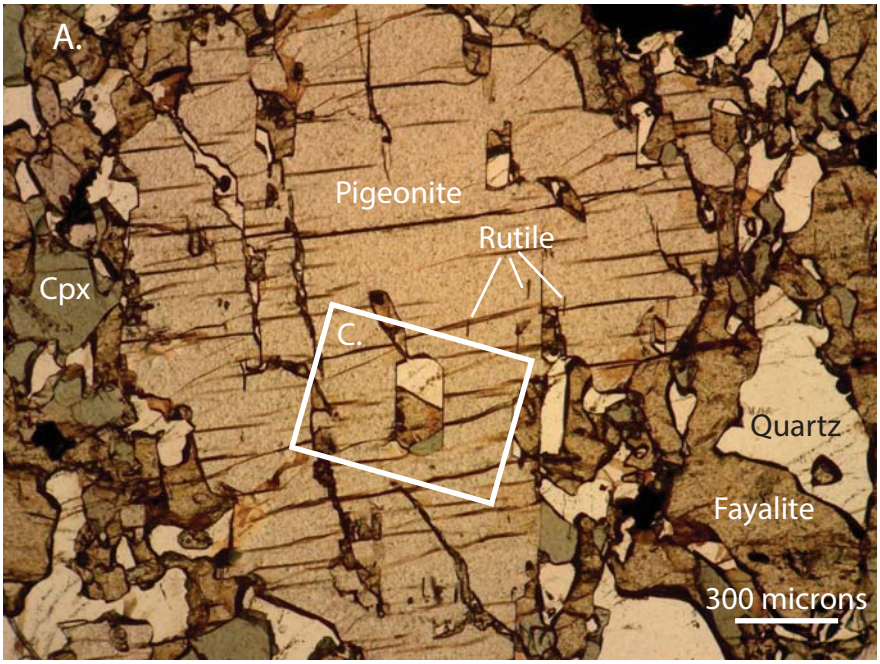
A.
Pigeonite
Rutile
Cpx
C.
Quartz
Fayalite
300 microns

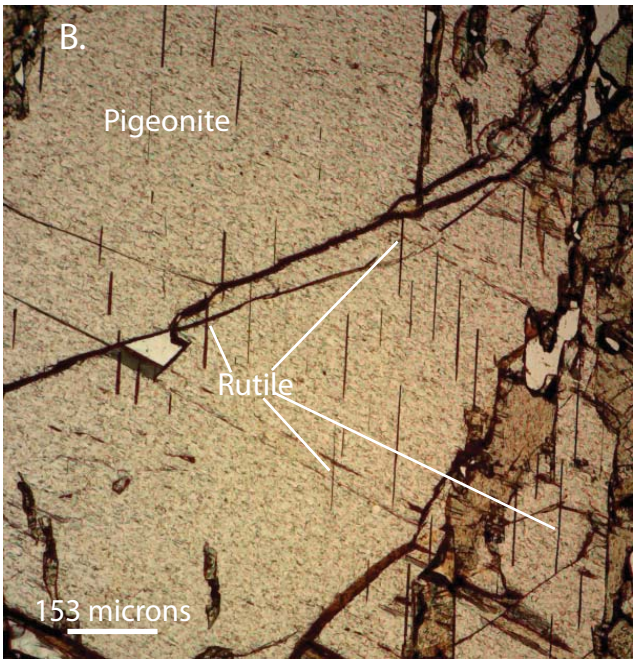
B.
Pigeonite
Rutile
153 microns

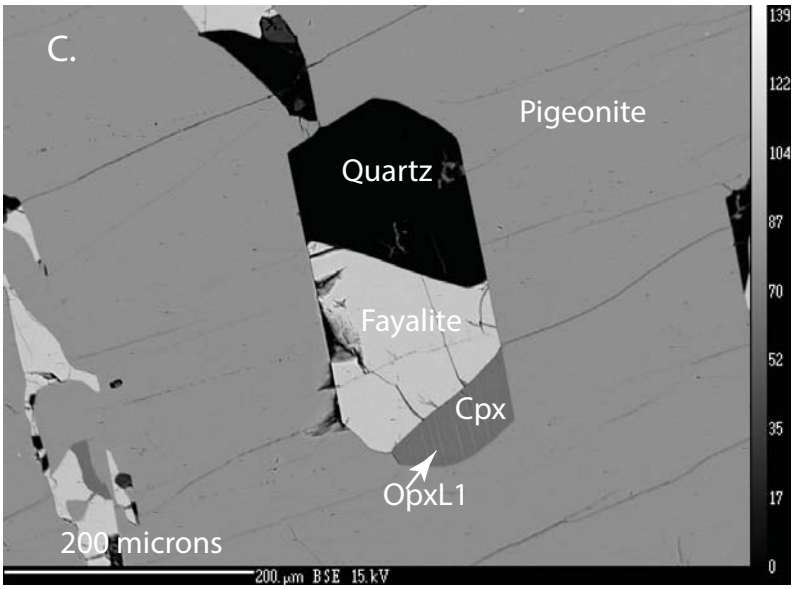
C.
Pigeonite
Quartz
Fayalite
Cpx
OpxL1
200 microns
200 µm BSE 15 kV
139
122
104
87
70
52
35
17
0

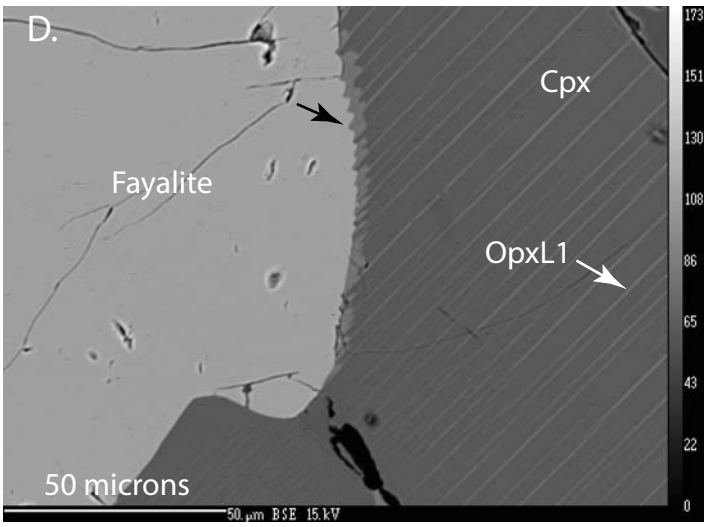
D.
Cpx
Fayalite
OpxL1
50 microns
50 µm BSE 15 kV
173
151
130
108
86
65
43
22
0

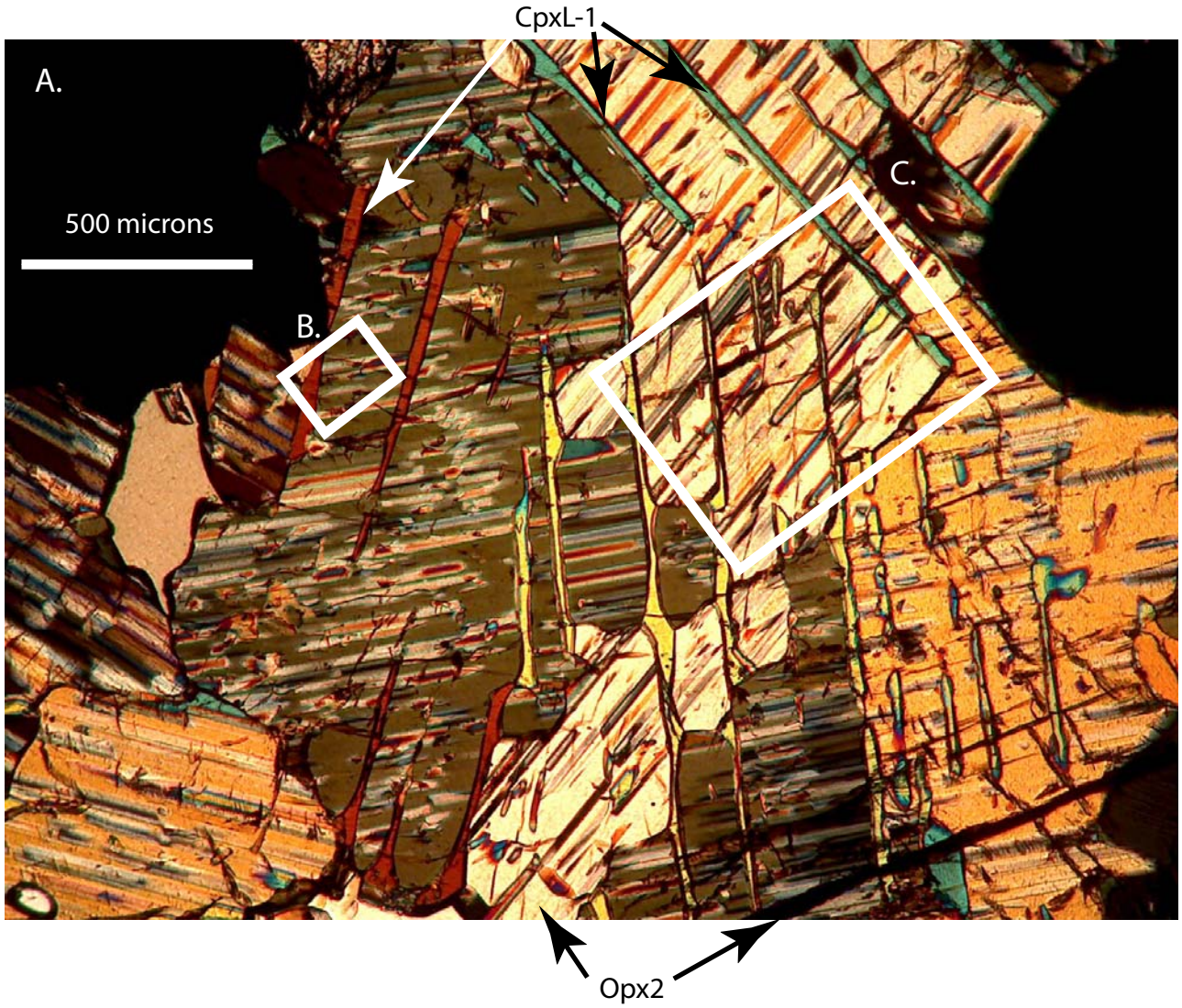
CpxL-1
A.
500 microns
B.
C.
Opx2

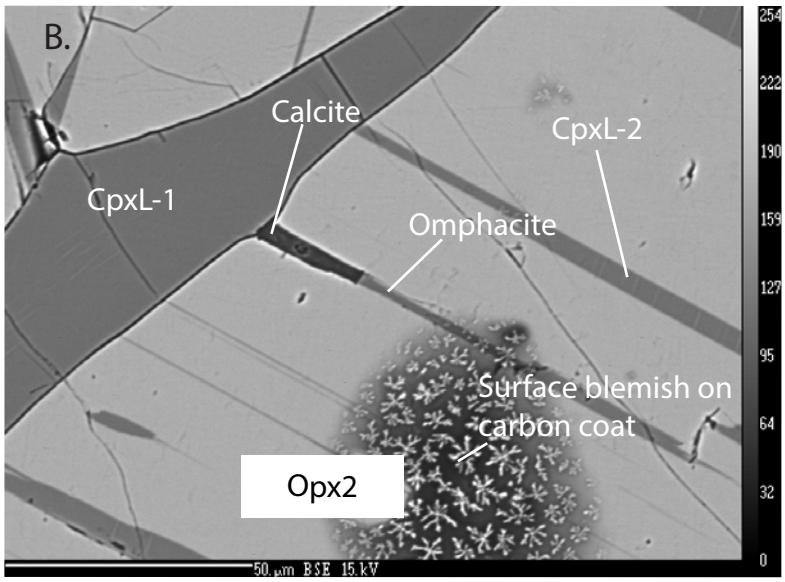
B.
Calcite
CpxL-2
CpxL-1
Omphacite
Surface blemish on carbon coat
Opx2
50 µm BSE 15 kV

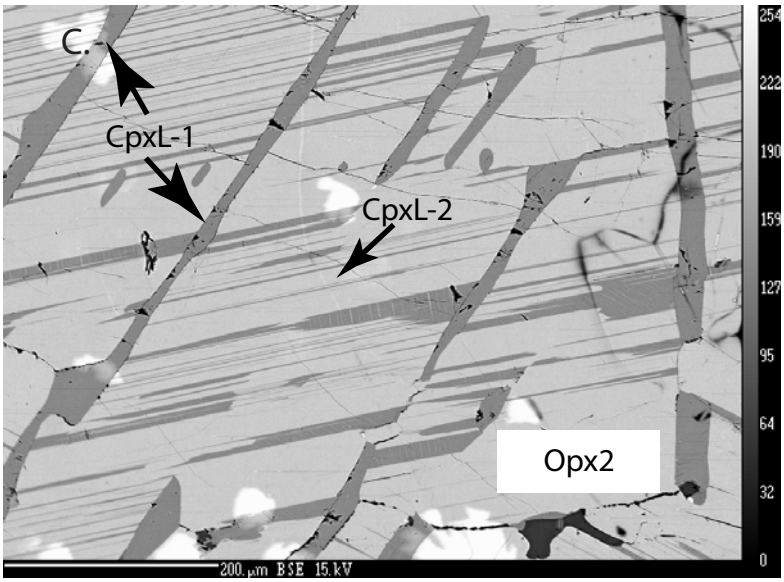
C.
CpxL-1
CpxL-2
Opx2
200 µm BSE 15 kV

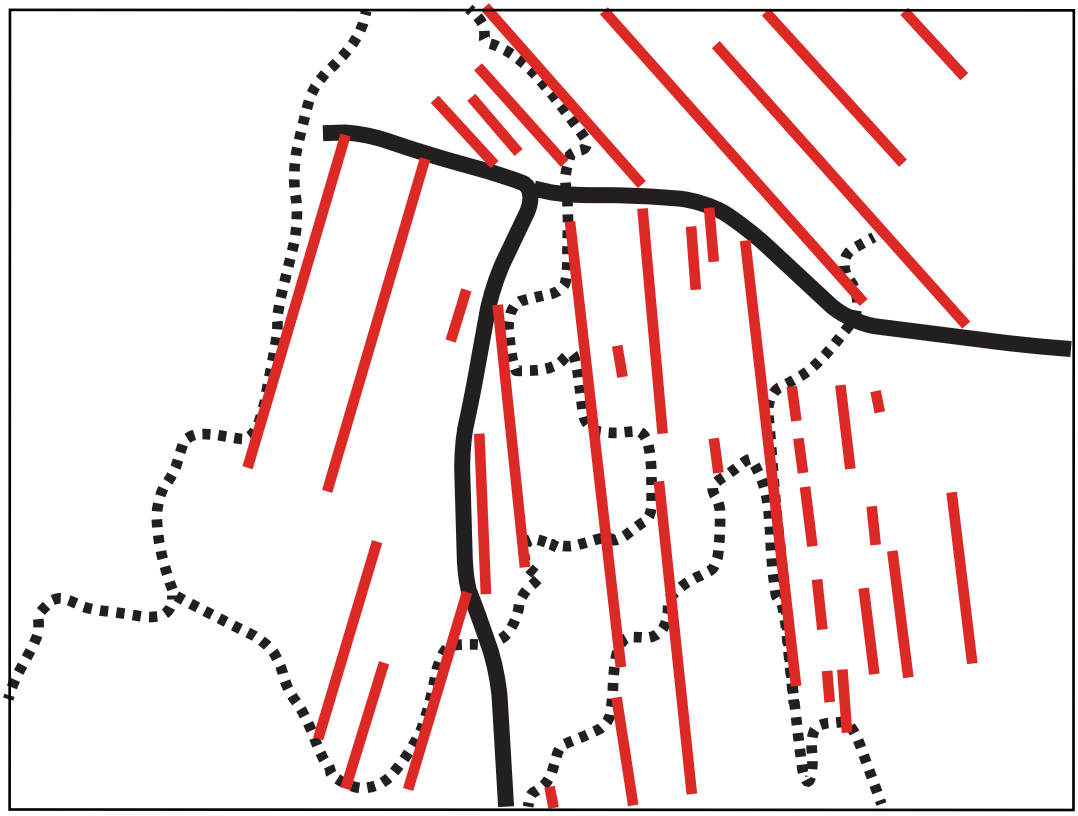
500 microns

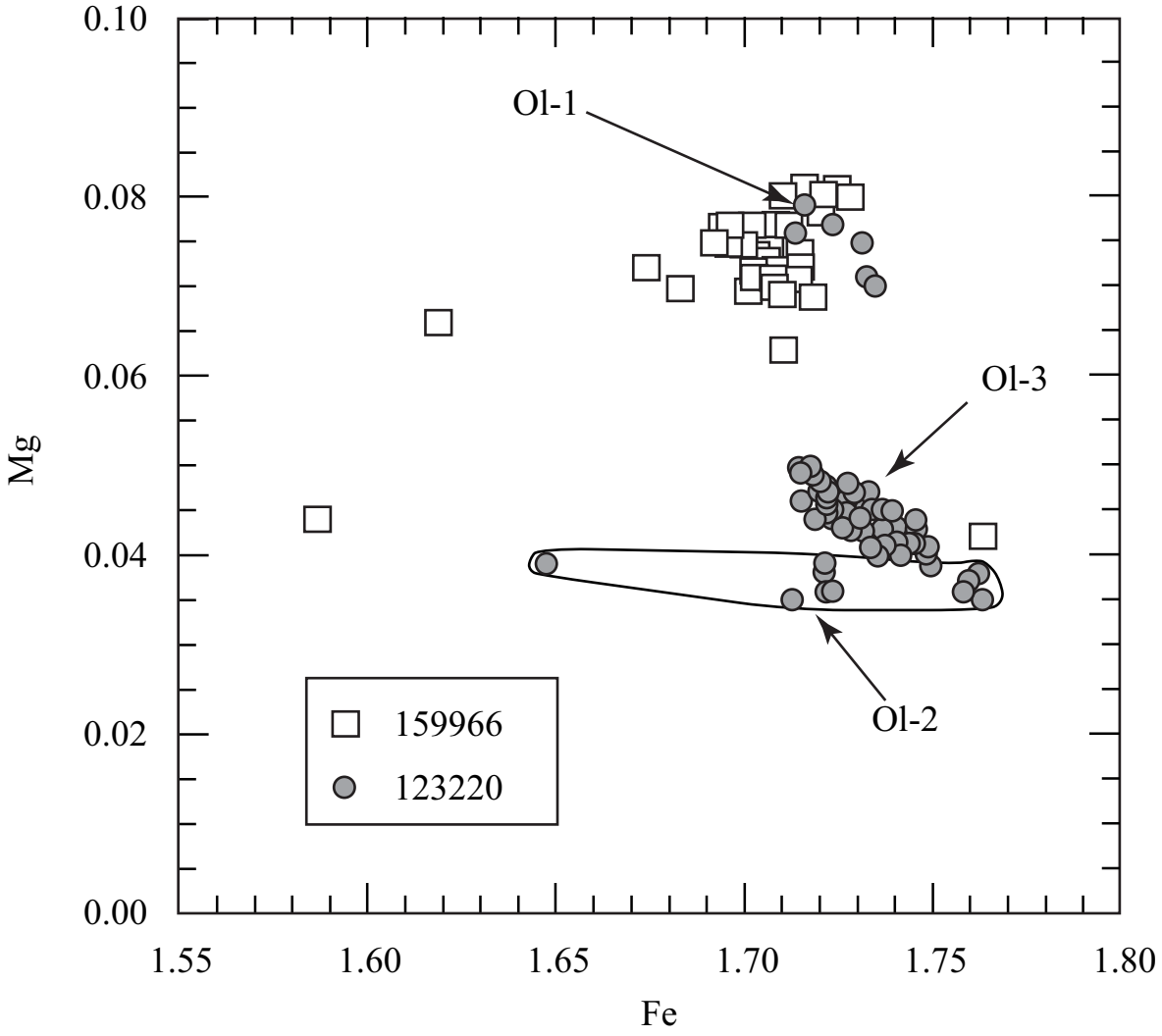

Glassley et al., West Greenland UHP *Figure 15*

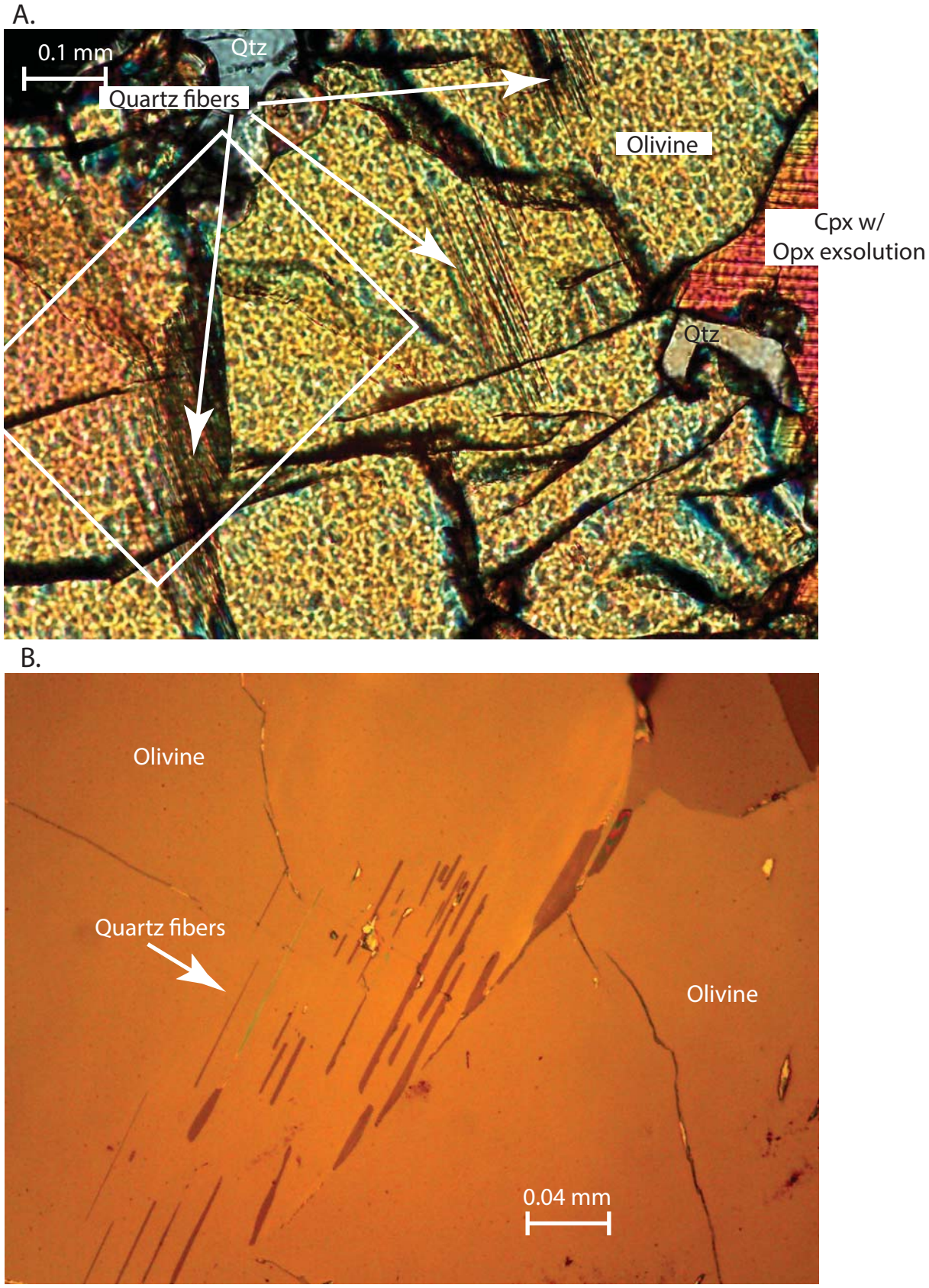
A.
0.1 mm
Qtz
Quartz fibers
Olivine
Cpx w/
Opx exsolution
Qtz
B.
Olivine
Quartz fibers
Olivine
0.04 mm

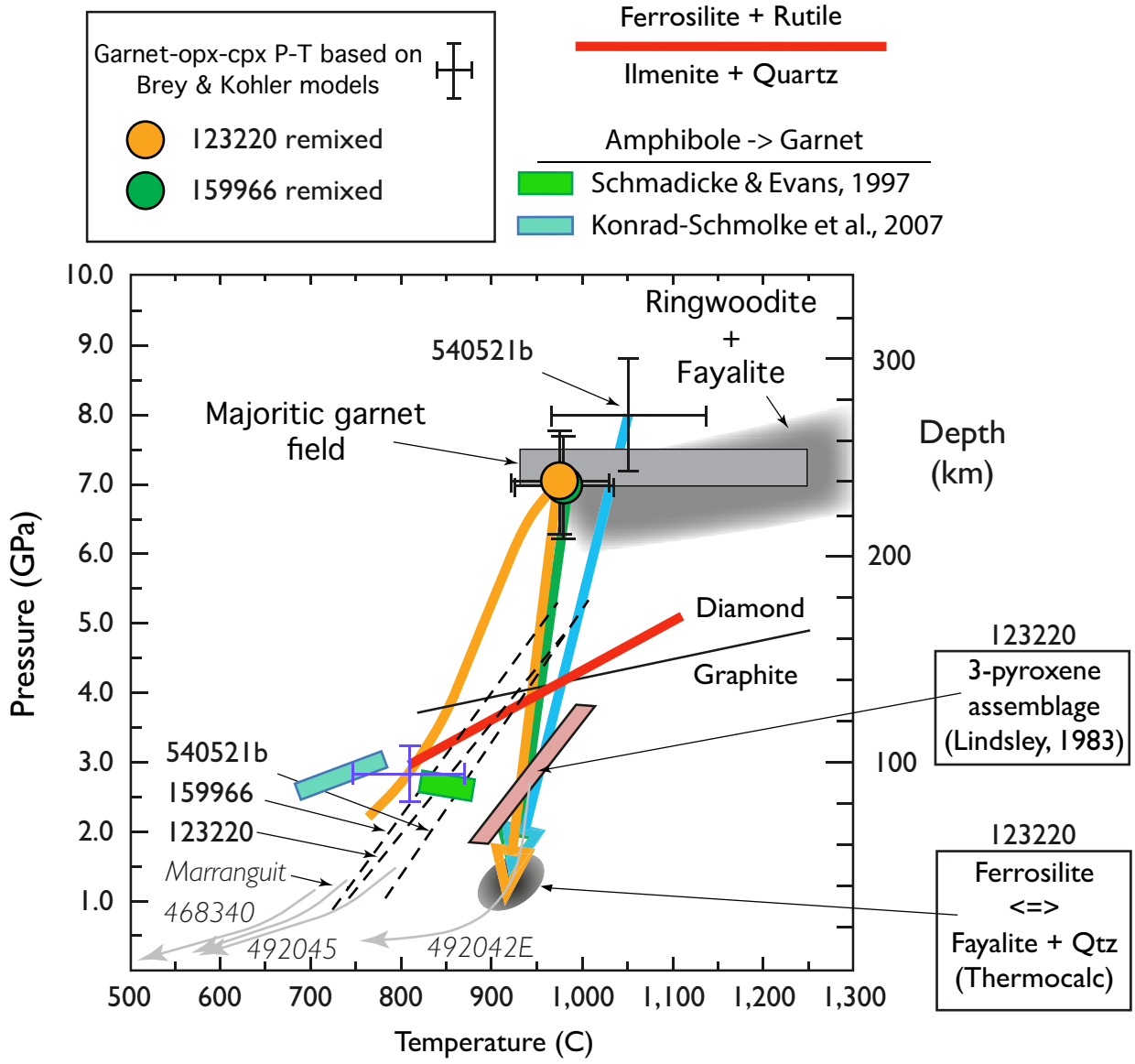

Glassley et al., West Greenland UHP *Figure 17*

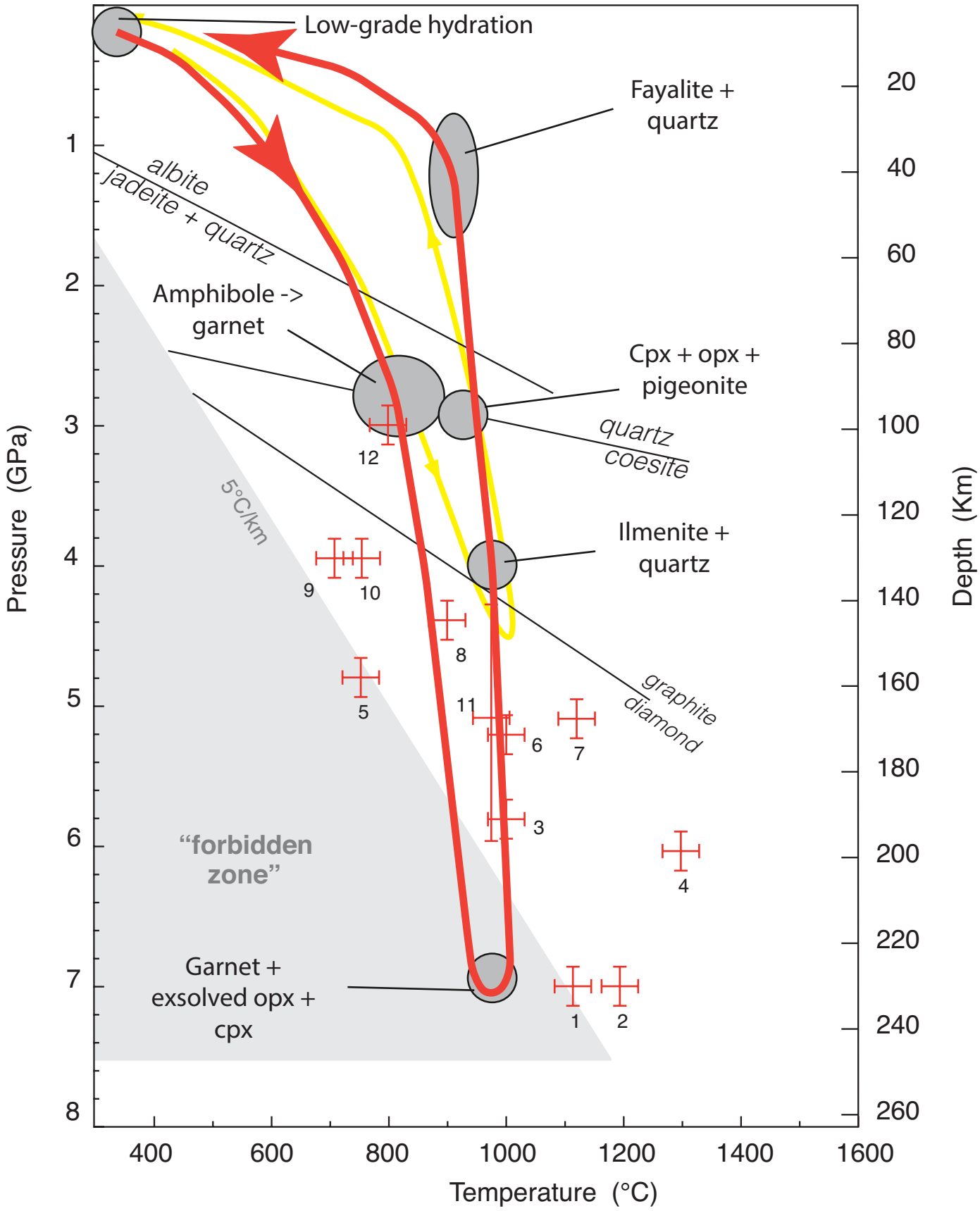

Glassley et al., West Greenland UHP

Figure 18

	123220 garnet core	123220 garnet mantle	123220 garnet rim	123220 garnet e-mixed (6% Opx	123220 Opx inclusion re-mixed	159966 garnet core	159966 garnet mantle
SiO2	37.17	37.20	37.27	37.14	39.05	37.23	36.99
TiO2	0.04	0.03	0.02			0.05	0.05
Al2O3	19.91	20.22	20.12	18.73	0.30	19.77	19.61
FeO	27.06	26.82	24.74	28.05	56.04	25.24	24.97
MgO	0.23	0.24	0.21	0.26	0.59	0.56	0.55
MnO	9.63	9.98	11.72	9.75	3.87	11.42	11.36
CaO	6.57	6.47	6.60	6.08	0.15	6.09	6.15
Na2O							
K2O							
Cr2O3	0.078	0.036	0.02			0.033	0.018
Cl							
Total	100.69	100.994	100.704	100.01	100	100.389	99.7
Si	3.02	3.01	3.02	3.04	3.53	3.03	3.03
Ti	0.003	0.002	0.001			0.003	0.003
Al	1.9	1.93	1.92	1.8	0.04	1.89	1.89
Fe2+	1.84	1.81	1.68	1.92	3.96	1.72	1.71
Mg	0.03	0.03	0.03	0.03	0.09	0.07	0.07
Mn	0.66	0.68	0.8	0.68	0.36	0.79	0.79
Ca	0.57	0.56	0.57	0.53	0.02	0.53	0.54
Na							
K							
Cr	0.005	0.003	0.001			0.002	0.001
O=	12	12	12	12	12	12	12
ppm by LAICPMS				S.D.			

Cr	414	128	185.3	5
V	383	385	389	10
Zn	6.93	6.99	6.78	0.6
Y	235	233	238.7	10
Nb	0.044	0.018	0.033	0.006
Ba	0.007	0.031	0	0.2
La	0.0041	0.085	0.013	0.008
Ce	0.109	0.239	0.082	0.01
Pr	0.057	0.0492	0.043	0.01
Nd	1.017	0.69	0.83	0.08
Sm	2.12	1.79	1.66	0.2
Eu	1.254	1.119	1.02	0.07
Gd	9.92	8.95	9.19	0.5
Tb	2.88	2.74	2.77	0.2
Dy	29.2	27.7	29.35	2
Ho	8.71	8.49	8.63	0.3
Er	29.36	29.4	29.6	1
Tm	4.27	4.36	4.47	0.2
Yb	29.6	29.4	29.4	1.5
Lu	3.98	4.2	4.08	0.2

159966 garnet rim	159966 Opx Ave	159966 Cpx Ave	159966 garnet e-mixed (6% Opx	159966 Opx inclusion re-mixed	540521b garnet core	540521b garnet mantle	540521b garnet rim
37.48	46.42	48.37	37.68	45.96	37.37	37.28	37.13
0.05		0.07			0.05	0.03	0.04
20.10	0.22	0.36	18.42	0.39	20.37	20.38	20.42
24.18	42.21	28.40	26.50	47.79	27.00	26.23	24.10
0.44	3.80	3.50	0.64	1.39	1.30	1.29	0.66
12.11	6.47	4.09	10.94	3.82	9.16	9.17	11.26
6.27	1.40	15.59	5.82	0.65	4.99	5.30	6.23
		0.13					
0.031		0.002					
100.664	100.52	100.512	100	100	100.235	99.683	99.837
3.03	1.97	1.98	3.08	1.99	3.03	3.02	3.01
0.003		0.002			,002	0.002	0.002
1.91	0.01	0.02	1.8	0.02	1.93	1.95	1.95
1.64	1.5	0.98	1.81	1.73	1.82	1.78	1.64
0.05	0.24	0.21	0.07	0.09	0.16	0.16	0.08
0.83	0.23	0.14	0.77	0.14	0.63	0.63	0.77
0.54	0.06	0.68	0.51	0.03	0.43	0.46	0.55
		0.01					
0.002		0					
12	6	6	12	6	12	12	12

540521b Opx integrated	540521b Cpx integrated	540521b Cpx Coarse lamellae	540521b Cpx Omphacite	123220 Bulk rock Wt. % (Fe2O3)	540521 Bulk rock Wt. % (Fe2O3)
47.68	49.34	49.77	45.27	43.10	48.30
0.1	0.12	0.11	0.70	0.04	0.17
0.45	0.78	0.71	10.73	0.46	2.83
33.88	22.29	21.76	25.17	46.85	34.86
5.65	5.21	5.37	5.23	0.95	4.96
4.76	2.94	2.51	1.20	7.27	4.78
5.66	17.75	19.94	10.55	3.60	3.89
0.09	0.24	0.21	1.69	<0.02	<0.02
				<0.02	<0.02
		0.01			
98.27	98.67	100.39	100.54	102.27	99.79
1.99	1.99	1.98	1.77		
0.003	0.004	0.003	0.02		
0.02	0.04	0.03	0.5		40 10 15 15 20 0
1.19	0.75	0.72	0.72		
0.35	0.31	0.32	0.31		
0.17	0.1	0.08	0.04		
0.25	0.77	0.85	0.44		
0.008	0.02	0.02	0.13		
6	6	6	6		